February 2010
Ph D
A study on the Welding Fracture Toughness of the ultra thick High-tensile Steel Plate(EH36-TMCP)
Seong-Joo KIM

February 2010
Ph.D Thesis

A study on the Welding Fracture Toughness of the ultra thick High-tensile Steel Plate(EH36-TMCP)

Graduate School of Chosun University

Department of Naval Architecture and Ocean Engineering

Seong-Joo Kim

A study on the Welding Fracture Toughness of the ultra thick High-tensile Steel Plate(EH36-TMCP)

극후판 고장력강(EH36-TMCP)의 용접부 파괴인성에 대한 연구

February 25, 2010

Graduate School of Chosun University

Department of Naval Architecture and Ocean Engineering

Seong-Joo Kim

A study on the Welding Fracture Toughness of the ultra thick High-tensile Steel Plate(EH36-TMCP)

Advisior: Professor Han-Sur Bang

A thesis submitted for the
Degree of Doctor of Philosophy in Engineering

February 25, 2010

Graduate School of Chosun University

Department of Naval Architecture and Ocean Engineering

Seong-Joo Kim

C O N T E N T S

ABSTRACT

A study on the Welding Fracture Toughness of the ultra thick High-tensile Steel Plate(EH36-TMCP)

Kim Seong-Joo
Advisor: Prof. Bang Han-Sur
Department of Naval Architecture & Ocean Engineering
Graduate School of Chosun University

For the promotion of structural integrity and pursuit of economical interest on large welding construction and operation of the construction, the thorough and rigorous evaluation and working control are an essential precondition to prevent the safety concern during the manufacturing and operating the construction. Considering the benefit from economics of scale is important, many large welding constructions such as offshore structures, VLCCs (Very Large Oil Carriers), VLOCs (Very Large Ore Carriers) and even container ships have been constructed and this trend may be maintained continuously in future.

In case of large container ships, this trend has been applied actively, and actually the size of the ship is being continuously increased. Along with this trend, the applications of thick steel plates with high strength (EH36-TMCP) that exceed more than 70mm and 355N/mm^2 in thickness and yield strength respectively are increased rapidly to satisfy the deduction of lightweight and increase of longitudinal strength of the ship.

The application of these thick steel plates, however, cause an advance in workload and man-hours to be invested for welding processes, accordingly the necessity of more efficient welding process by using the large heat input welding i.e. EGW (Electro Gas Welding) are raised to the cost-reduction, instead of using the conventional semi-automatic FCAW (Flux Cored Arc Welding).

But, the application of the EGW as an efficient welding process causes to increase the brittleness on the welding region because of large heat input, and resultantly the fracture

toughness of welding materials may be affected, comparing with an application of ordinary multi-layer FCAW welding. Considered the assurance of fracture toughness on thick steel plates with high strength is indispensible to the large welding construction, the characteristics of EGW need to be investigated and furthermore the effectiveness of the using EGW as a substitution of FCAW also needs to be verified for applying the thick steel plates with high strength (EH36-TMCP).

For the purpose of this, the analyses for welding residual stress are conducted to the FE models which have been welded by EGW and FCAW respectively. And, for consideration of actual working condition, the redistributed welding residual stresses, when the external bending load and initial crack are induced, are re-analyzed on the basis of the conducted FE analyses for welding residual stress.

Acknowledging the fracture toughness is the most important factor among the large welding constructions to which the thick steel plates with high strength are used, the analyses of fracture toughness for each welding process i.e. EGW and FCAW are conducted in this study and the result shows that the fracture toughness (K_{IC}) for the EGW, which is considered as a terms of crack initiation, is lower than FCAW. But, it is considered to negligible as the difference of the toughness values between two welding processes is very small compared with mechanical properties of welding materials.

For the confirmation of mechanical characteristics and integrity after welding, the mechanical experiments have been carried out and it is confirmed that the properties are complied with the classification rules for EH36-TMCP. As a verification of fracture toughness in way of welding regions, CTOD test in accordance with British standard BS 7448 and the review of fractured surfaces by SEM(Scanning Electron Microscope) have been carried out. The result shows that the FCAW have higher value than EGW in CTOD value and the fractured surfaces show that ductile fracture in FCAW and cleavage fracture in EGW have been occurred.

Conclusively, the analyses and experimental result shows that characteristics of EGW have been slightly deteriorated compared with FCAW but the result can be acceptable to the concerned thick plates with high strength, EH36-TMCP as an substitution of conventional multi-layer welding, FCAW.

List of Figure

List of Table

List of Photo.

Chapter 1. Introduction

1.1 Purpose of this study

For the pursuit of economical benefits in terms of reduction in initial cost-investment, the ships have become larger than conventional types and this trend is remarkable in container ships[1-4]. Along with this trend for large sized ships, above 8,000TEU container ships in particular, the application of thick steel plates with high strength having yield strength and thickness higher than 355N/mm^2 and 70mm respectively has increased rapidly to satisfy the deduction of lightweight and increase the longitudinal strength of the ships[5-8].

The application of these ultra thick steel plates with high strength, however, may make high demands on the workload for welding, thus the necessities of the high efficient manufacturing processes in welding such as one pole EGW(Electro gas Welding) for 55mm below in thickness, and two pole EGW or one pole & FCAW(Flux Cored Arc Welding) for 55mm above in thickness, are increased to overcome the difficulties encountered for conventional multi-layer welding process such as semi-automatic arc welding, FCAW[9-13].

As the EGW which is an automatic welding for time saving is a welding process with large heat input, however, the mechanical properties in welding zone including heat affected zone(HAZ) may be affected with possibility of brittle fracture, furthermore crack susceptibility may be increased than ordinary multi layer welding process. Therefore, these kinds of thick steel plates which were welded by large heat input need to be treated by post heat treatment for the prevention of further brittle fracture at service stage, even need a control of heat input[9-13].

Additionally, in accordance with a standard of offshore construction, the post heat treatment to increase fracture toughness or CTOD test to confirm the integrity of the welding construction are required to the offshore steel construction if the heat input of welding and thickness of the structure are more than 45KJ/cm^2 and 50mm respectively[14-15].

Acknowledging these deterioration in terms of the fracture toughness and fatigue life on the ultra thick steel plates with high strength, which have been used in the large-sized welding constructions, some classification societies consider to apply the relevant requirements to reinforce the integrity of welding constructions and estimate the fracture toughness of the construction by means of CTOD(Crack Tip Opening Displacement) test or Kca(crack arrest ability), for instance, the Requirement of CTOD estimation for offshore structure steel($\geq$ 45mmt) by DNV, the Requirement of CTOD estimation for heavy TMCP steel(72/88mmt) for container carrier by NK and the Requirement of crack arrestability(Kca) assurance for heavy thick plate(50-100mmt) by NK(July 2006).

Therefore, considering the study and relevant verification for mechanical properties and fracture behaviors are indispensible to ensure the integrity, soundness and durability in welding constructions, the analyses to predict the temperature variation and welding residual stress by heat conduction and to investigate the fracture behavior by welding residual stress have been conducted by the EGW in this study, and the characteristics of EGW have been compared with those of FCAW.

In order to achieve this purpose, the FEM analyses to non-liner heat conduction and mechanical behaviors have been carried out by developed in-house solver considering the temperature dependency of the welding materials such as heat conduct, specific heat, density and the mechanical properties such as yield stress, modulus of elasticity, coefficient of thermal expansion and others. Additionally, for further analysis for plain strain fracture toughness(K_{IC}) in way of the notch, the stress intensity factors have been calculated for the residual stress and a residual stress superposed with bending load by a commercial FE solver, ANSYS to which the welding residual stress calculated by in-house solver was used as a external load.

The theoretical analyses for the each welding process, EGW & FCAW, have been verified by experimental examinations by which mechanical properties such as tensile, bending, impact and CTOD, and also micro structural inspection by SEM(Scanning Electron Microscope) have been examined. Finally, the credibility of each welding process, EGW in particular, has been confirmed by theoretical and experimental analyses.

1.2 Contents and analytical method followed in this study

During the welding, thermal stress due to the uneven temperature distribution occurs and after the welding, occurrence of the welding residual stress by non-liner plastic strain is inevitable. This welding residual stress may deteriorate the credibility and safety of welding constructions during the manufacturing and also service stage, accordingly this welding residual stress shall be dealt thoroughly in terms of the maintaining the safety and sound welding constructions.

Recognized the tensile welding residual stress remaining on the center layer of welding can exert to decrease the fatigue strength due to the increase of possible crack propagation and also to decrease the resistibility against to brittle fracture, the exact evaluation of welding residual stress is important to fracture behaviors of welding structures being affected by welding residual stress.

Furthermore, when existed welding residual stress are superposed with external load, a brittle fracture at less stress than specific yield stress may occur on the welding construction. Therefore, thorough examination and analysis for the welding residual stress regarding the fracture aspects is very important to the welding construction.

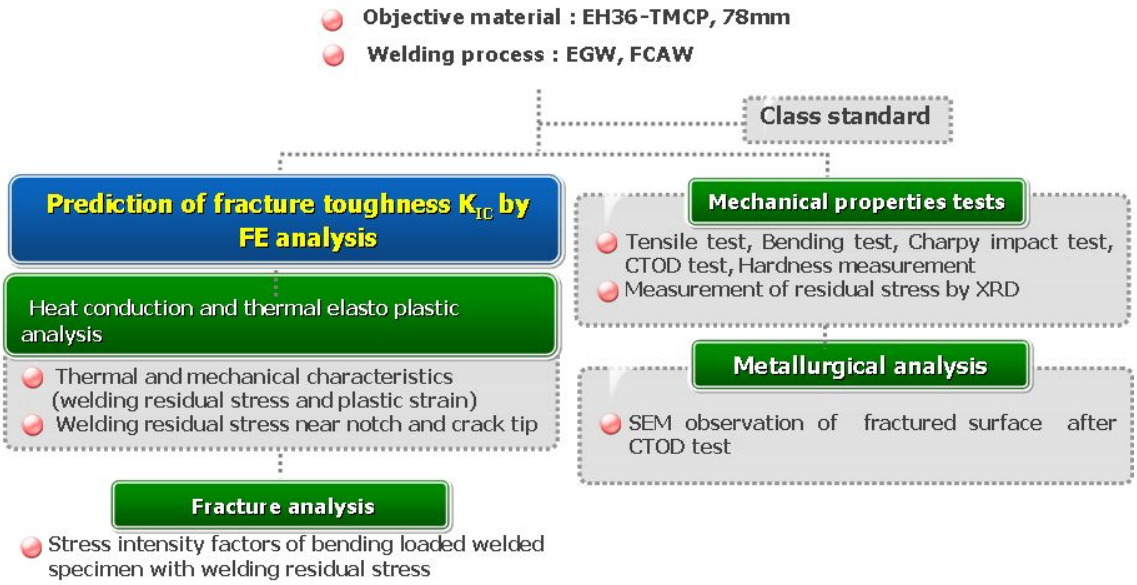

Fig. 1.1 Research methodologies

In this study, following three procedures for welding heat conduction, residual stress and fracture analysis were conducted to investigate the fracture toughness K_{IC} for high strength ultra thick plate(EH36-TMCP) by the variation of welding processes, EGW and FCAW, as shown Fig 1.1 and 1.2 [16-22]:

1) Analysis of heat conduction: temperature distribution by time dependent
2) Analysis of welding residual stress: thermal stress, residual stress and strain by the uneven temperature distribution
3) Analysis of fracture behavior: plain strain fracture behavior by residual stress superposed with an external load

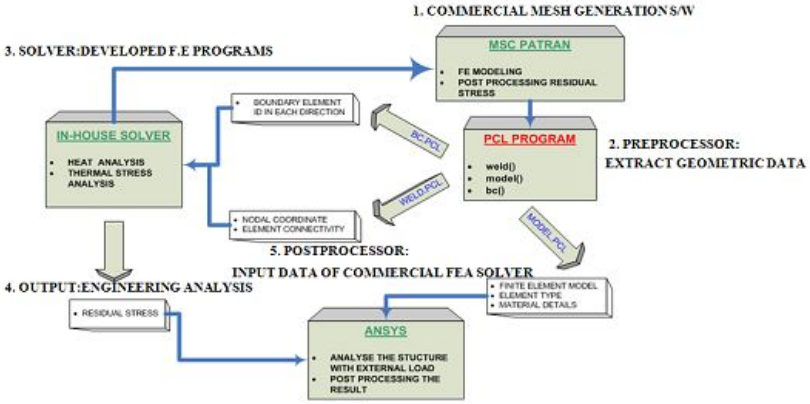

Fig. 1.2 Flowchart for transferring input data between in-house and commercial solver

In the study, the analyses have been conducted by the in-house FE solver which was developed considering the two-dimensional heat conduct and the plain strain thermal elastic-plastic theories and as a pre- and post processor the commercial FE processor, MSC PATRAN, is used.

Additionally, FEM code by in-house solver has been applied as the initial loading case in the welded structure and analysis has been carried out using commercial package(ANSYS). The mechanical properties for this analysis consider the dependency of temperature change on both elastic & plastic region, and plastic-flow theory is adapted in the plastic region.

After completion of the analysis for heat conduction and thermal stress, the redistribution of welding residual stress and plain strain fracture toughness K_{IC} have been considered by commercial package(ANSYS).

As verification means of these analyses through the experimental test, the welding specimens were manufactured as same with actual FE model and same condition such as shape, dimensions and welding condition. Comparing the FE analyses with experimental results, i.e. by measurements of welding residual stress and by test for mechanical properties (tensile, bending and impact and review of SEM), the mechanical characters and FE analyses for welding regions have been reviewed to confirm the pertinence. Furthermore, CTOD test by using 3-point bending test has been carried out to confirm the result of fracture toughness in way of fusion line where lowest level of fracture toughness may be occurred [23-25].

Chapter 2. Numerical Analysis to investigate the welding characteristics

2.1 Basic theory for heat transfer analysis

In this study, the effect of heat source has been considered to conduct the definite analysis and the two dimensional 4-node iso-parametric elements also have been induced to progress the accuracy of analysis by using the natural coordinate system. Considering the temperature distribution that is changed by time elapsed, the FEM analyses to non-liner heat conduction and mechanical behaviors have been carried out by self-developed in-house solver considering the temperature dependency of the welding materials such as heat conductivity, specific heat and density.

On the basis of above-mentioned theory, the governing equation for un-stationary heat conduction has been described as follows:

$$q = -\lambda_x \frac{dT}{dx} \tag{2.1}$$

So for 2D-case the rate of heat transfer is

$$\frac{\partial}{\partial x}(\lambda_x \frac{\partial T}{\partial x}) + \frac{\partial}{\partial y}(\lambda_y \frac{\partial T}{\partial y}) \tag{2.2}$$

The thermal analysis has been conducted using temperature dependent thermal material properties and from conservation of energy the governing equation of heat conduction in weldment is obtained on the conception of the medium to be isotropic, as follows:

$$\rho c \frac{\partial T}{\partial t} = \lambda(\frac{\partial^2 T}{\partial x^2} + \frac{\partial^2 T}{\partial y^2}) + Q \tag{2.3}$$

where, ρ is Density, c is specific heat, λ is heat conductivity, T(x, y, z, t) is temperature at certain space(x, y, z) at certain time t and Q is heat input.

The model to be analyzed is created and then discretized into finite number of elements and insert the relation between element temperature T(x,y,t) of certain time, *t* and nodal temperature vector of finite element, $\{\phi(t)\}$ using shape function [N] as follow:

$$T(x, y, t) = [N(x, y)]\{\phi(t)\}$$

And then applying the Galerkin method (weighted residual method) that put the shape function [*N*] as weighted function to (2.3) become as follows:

$$\int_{V^e} [N]^T \left\{ \lambda \left(\frac{\partial^2 T}{\partial x^2} + \frac{\partial^2 T}{\partial y^2} \right) + Q - \rho c \frac{\partial T}{\partial t} \right\} dV = 0 \tag{2.4}$$

And then partially integrating (2.4),

$$\int_{V^e} \left\{ \lambda \left(\frac{\partial [N]^T}{\partial x} \frac{\partial [T]}{\partial x} + \frac{\partial [N]^T}{\partial y} \frac{\partial [T]}{\partial y} \right) + [N]^T \rho c \frac{\partial T}{\partial t} + \right\} dV$$

$$= \int_{s^e} \lambda [N]^T \frac{\partial T}{\partial n} dS + \int_{V^e} Q [N]^T dV \tag{2.5}$$

Applying the error distribution principal known as Galerkin method, and setting the n-integral form to zero and then applying Green-Gauss theorem the elemental formulation can be finally written as (2.6).

$$[K]\{\phi\} + [C]\left\{ \frac{\partial \phi}{\partial t} \right\} = \{F\} \tag{2.6}$$

Where Conductance matrix,

$$[K] : \int_{V^e} \lambda \left(\frac{\partial [N]^T}{\partial x} \frac{\partial [N]}{\partial x} + \frac{\partial [N]^T}{\partial y} \frac{\partial [N]}{\partial y} \right) dV \tag{2.7}$$

Heat capacity matrix,

$$[C] = \int_{V^e} \rho c [N]^T [N] dV \tag{2.8}$$

Load vector,

$$\{F\} = \int_{s^e} q [N]^T dS + \int_{V^e} Q [N]^T dV \tag{2.9}$$

Using this formulation the finite element code has been developed for the heat transfer analysis consisted with 28 subroutines and according to the task performed, subroutines can be grouped accordingly as shown in the block diagram of Fig. 2.1.

2.2 Nonlinear thermal elastic-plastic analysis

The solid has been assumed to be isotropic medium for welding residual stress analysis and mechanical properties of material are dependent on temperature change in both elastic and plastic region. Plastic-flow theory is adopted in the plastic region. Relation between strain and displacement is described as follow.

$$\{ d\varepsilon \} = [A]\{ dU\} \tag{2.10}$$

where $\{dU\}$ is increment of element displacement, matrix $[A]$ contains the differential operator.

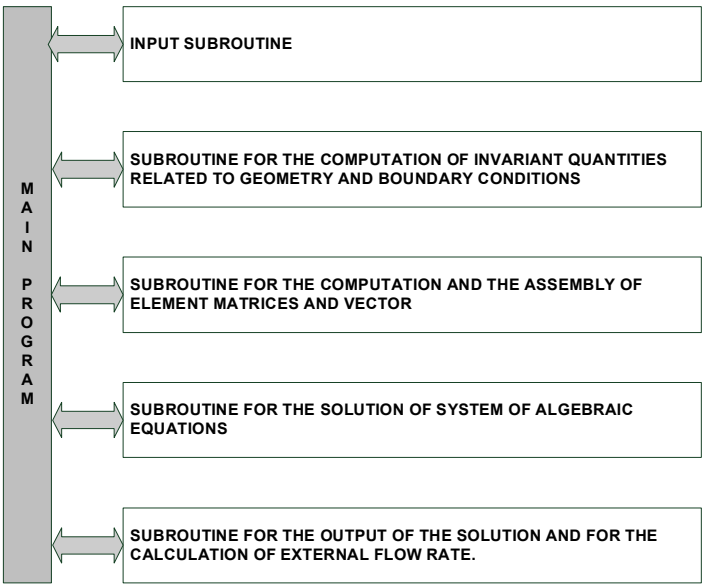

Fig. 2.1 Structure of the Heat transfer analysis program

By using shape function $[N]$ which connects between nodal displacement and element displacement, increment of nodal displacement is as follow.

$$\{ dU\} = [N]\{ dw\} \tag{2.11}$$

Using element strain-displacement relation matrix, $[B]=[A][N]$ then the relation between nodal displacement increment and element displacement increment are as follows referring to (2.10) and (2.11).

$$\{ d\varepsilon \} = [A][N]\{ dw\} = [B]\{ dw\} \tag{2.12}$$

When $[D^e]$ is the elastic stress-strain matrix, $\{\alpha\}$ as linear expansion coefficient, then stress-strain relation in elastic region is given by

$$\{d\sigma\} = [D^e]\{d\varepsilon\} - [D^e]\left(\frac{\partial [D^e]^{-1}}{\partial T}\{\sigma\} + \{\alpha\}\right)dT \tag{2.13}$$

Above relation is simply expressed as,

$$\{d\sigma\} = [D]\{d\varepsilon\} - \{C\}dT \tag{2.14}$$

Where $[D] = [D^e]$, $\{C\} = [D^e]\left(\frac{\partial [D^e]^{-1}}{\partial T}\{\sigma\} + \{\alpha\}\right)dT$.

Considering plastic strain increment theory and using yield function as plastic potential, plastic strain increment, $\{d\varepsilon^p\}$ is

$$\{d\varepsilon^p\} = d\lambda\left\{\frac{\partial f}{\partial \sigma}\right\} \tag{2.15}$$

Where $d\lambda$ is as follows

$$d\lambda = \frac{\left\{\frac{\partial f}{\partial \sigma}\right\}^T [D^e]\{d\varepsilon\} - \left\{\frac{\partial f}{\partial \sigma}\right\}^T [D^e](\{\alpha\} + \frac{\partial [D^e]^{-1}}{\partial T}\{\sigma\})dT + \frac{\partial f}{\partial T}dT}{\left\{\frac{\partial f}{\partial \sigma}\right\}^T [D^e]\left\{\frac{\partial f}{\partial \sigma}\right\} + \left\{\frac{\partial f}{\partial \varepsilon^p}\right\}\left\{\frac{\partial f}{\partial \sigma}\right\}} \tag{2.16}$$

Finally, stress-strain relation in plastic region is given by

$$\{d\sigma\} = [D^p]\{d\varepsilon\} - ([D^p]\{\alpha\} + [D^p]\frac{\partial [D^e]^{-1}\{\sigma\}}{\partial T}$$

$$+ \frac{[D^e]\left\{\frac{\partial f}{\partial \sigma}\right\}\left\{\frac{\partial f}{\partial T}\right\}}{\left\{\frac{\partial f}{\partial \sigma}\right\}^T [D^e]\left\{\frac{\partial f}{\partial \sigma}\right\} - \left\{\frac{\partial f}{\partial \varepsilon^p}\right\}^T\left\{\frac{\partial f}{\partial \sigma}\right\}})dT \tag{2.17}$$

Where plastic stress-strain matrix $[D^p]$ is

$$[D^p] = [D^e] - \frac{[D^e]\left\{\frac{\partial f}{\partial \sigma}\right\}\left\{\frac{\partial f}{\partial T}\right\}^T [D^e]}{\left\{\frac{\partial f}{\partial \sigma}\right\}^T [D^e]\left\{\frac{\partial f}{\partial \sigma}\right\} - \left\{\frac{\partial f}{\partial \varepsilon^p}\right\}^T\left\{\frac{\partial f}{\partial \sigma}\right\}} \tag{2.18}$$

Then (2.17) is simply expressed as following expression, similar to the elastic region's (2.14).

$$\{d\sigma\} = [D]\{d\varepsilon\} - \{C\}dT \tag{2.19}$$

Where $[D] = [D^p]$,

$$\{C\} = [D^p]\{\alpha\} + [D^p]\frac{\partial [D^e]^{-1}}{\partial T}\{\sigma\} + \frac{[D^e]\left\{\frac{\partial f}{\partial \sigma}\right\}^T\left\{\frac{\partial f}{\partial T}\right\}}{\left\{\frac{\partial f}{\partial \sigma}\right\}^T[D^e]\left\{\frac{\partial f}{\partial \sigma}\right\} - \left\{\frac{\partial f}{\partial \varepsilon^p}\right\}^T\left\{\frac{\partial f}{\partial \sigma}\right\}}$$

When the virtual displacement δ is given to discretionary body and the mechanical boundary condition S* is given along the boundary of discretionary body, the principle of virtual work is expressed as following ,

$$\int_v \{\delta(d\varepsilon)\}^T\{d\sigma\}dV - \int_v \{\delta(dU)\}^T\{d\overline{F}\}dV - \int_{S*} \{\delta(dU)\}^T\{d\overline{T}\}dS = 0 \tag{2.20}$$

Where volume of discretionary body is V, stress increment is $\{d\sigma\}$, strain increment is $\{d\varepsilon\}$, displacement increment is $\{dU\}$, body force per unit volume is $\{d\overline{F}\}$ and surface force per unit area is $\{d\overline{T}\}$. This equation is finally expressed as following finite element formula about one finite element of the model(body) if equation number (2.11), (2.12), (2.14) and (2.19) are inputted to (2.20).

$$[k]\{dw\} = \{f_v\} + \{f_s\} + \{f_T\} \tag{2.21}$$

Where [k] is stiffness matrix of element, $\{f_v\}$ is load vector of nodal point by body force, $\{f_s\}$ is load vector of nodal point by surface force and $\{f_T\}$ is equivalent nodal load vector by heat strain, which are expressed as below, respectively.

$$[k] = \int_{V_e} [B]^T[D][B]dV \qquad [f_v] = \int_{V_e} [N]^T[d\overline{F}]dV,$$

$$[f_s] = \int_{S_e} [N]^T[d\overline{T}]dS \qquad [f_T] = \int_{V_e} [B]^T(\{C\}dT)dV$$

Stress and strain of the whole model is obtained by solving above equations applying proper boundary conditions for each given problem. Using these formulations the finite element code has been developed for the residual stress analysis. The developed code consist of 47 subroutines and according to the task performed, subroutines can be grouped accordingly as shown in the block diagram of Fig. 2.2.

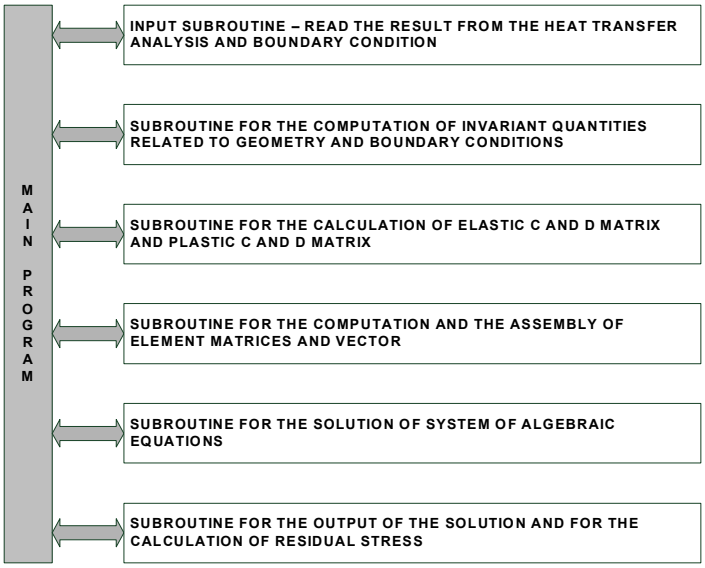

Fig. 2.2 Structure of the Residual stress analysis program

2.3 Fracture toughness (K_{IC})

The characteristics of material, such as tensile strength and fatigue strength, in which any existent crack is not existed, could be expressed by stress value, while the characteristics of crack induced material need to be described by an another index. When a crack exists in the materials, the fracture may rapidly propagate to the material from the crack tip as increasing the working loads such as external bending load or internal residual stress, and when this kind of unstable fracture is initiated, the resistance to withstand this crack initiation is considered to the fracture toughness for the materials. This fracture toughness can be described to stress intensity factor K_{IC} as an index of crack resistance and these two factors i.e. crack resistance and stress intensity factor K_{IC} have a same dimension.

When the relations between the stress and dislocation on any point in direction of crack tip regarding the fracture toughness factor are expressed by Fig.2.3, a distance (r) between crack tip & concerned point and dislocation of the point which is angled from crack face have following relations.

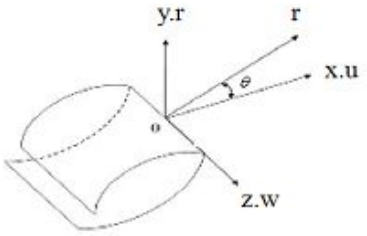

Fig. 2.3 Local coordinate system at the crack front and a point of crack tip vicinity

$$u=\frac{K_1}{4G}\sqrt{\frac{r}{2\pi}}[(2k-1)\cos\frac{\Theta}{2}-\cos\frac{3\Theta}{2}] \\ -\frac{K_2}{4G}\sqrt{\frac{r}{2\pi}}[(2k+3)\sin\frac{\Theta}{2}+\sin\frac{3\Theta}{2}+0(r) \tag{2.22}$$

$$v=\frac{K_1}{4G}\sqrt{\frac{r}{2\pi}}[(2k+1)\sin\frac{\Theta}{2}-\sin\frac{3\Theta}{2}] \\ -\frac{K_2}{4G}\sqrt{\frac{r}{2\pi}}[(2k+3)\cos\frac{\Theta}{2}+\cos\frac{3\Theta}{2}]+0(r) \tag{2.23}$$

$$w=\frac{2K_3}{G}\sqrt{\frac{r}{2\pi}\sin\frac{\Theta}{2}}+0(r) \tag{2.24}$$

where, 0(r) can be neglected due to very small value. As the G is shearing modulus, the Poisson's ratio ν is k=(3-ν)/(1+ν) on plain stress and k=(3-4ν) on plain strain.

When the $\Theta=0^{o}$, fracture toughness factor K and non-dimensional fracture toughness factor F regarding external load and superposed load with external & residual stress have been described as follows, and K_1 and K_2 mean the fracture toughness in opening mode and in-plane mode respectively as described on Fig.2.4.

$$K_1=\lim_{r\to 0}\sqrt{2\pi r}(\sigma_y\cos Q+\tau_{xy}\sin Q) \tag{2.25}$$

$$K_2=\lim_{r\to 0}\sqrt{2\pi r}(\tau_{xy}\cos Q-\sigma_y\sin Q)$$

$$F_1=K_1/\sigma\sqrt{\pi a},\ F_2=K_2/\sigma\sqrt{\pi a} \tag{2.26}$$

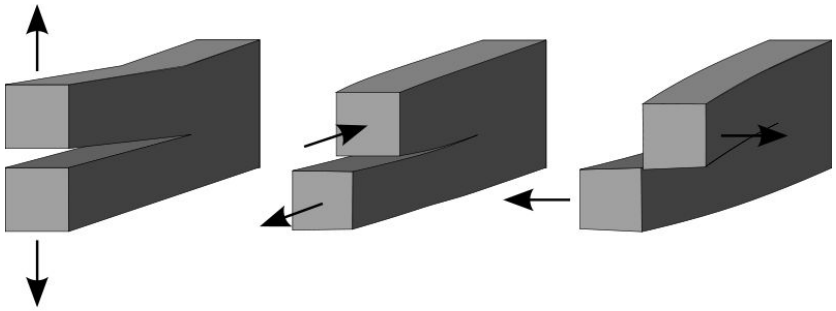

Fig. 2.4 Fracture Mode

Chapter 3. Heat conduction and stress analyses by welding processes

3.1 FE model and material properties

In this study, shipbuilding steel plate, EH36-TMCP (classification grade) as a FE model, being used to the large container ship, was assigned to analyze the large heat input welding(EGW), and existing multi-layer welding(FCAW).

The chemical composition and mechanical properties of the specimen and welding electrodes are described on Table.3.1 and 3.2, and in accordance with the WPQT of classification societies, the dimension was decided to 1,200mm in length, 400mm in breadth and 78mm in thickness. Reflected the field condition of welding, the shape and angle of welding groove were chosen the X shape in both sides, 30 degrees in bevel angle and 8mm in gap.

The details of welding joint shape, number of layer and other welding condition were shown on Fig.3.1, Table 3.3 & 3.4 respectively. FE model and mesh were determined to consider the character of temperature distribution and stress variation as shown on Fig. 3.2, and an initial notch in accordance with BS 7448 was inserted to the CGHAZ(Coarsened Grain Heat Affected Zone) adjacent to fusion line which is estimate to the weakest toughness region, to produce the quantitative toughness value around fusion line.

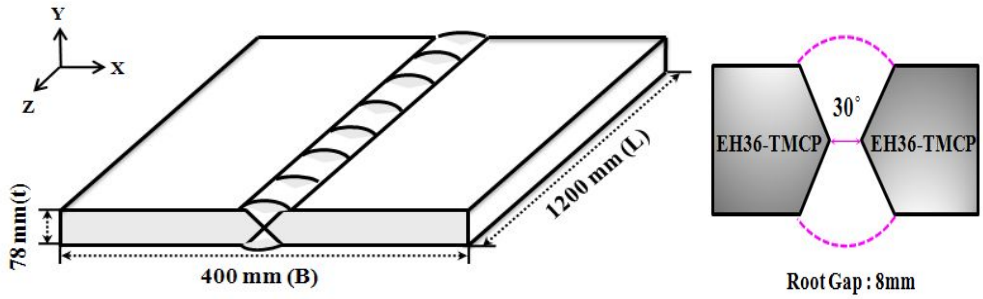

(a) Welded specimen and coordinate

(b) Cross section of EGW welded specimen

(c) Cross section of FCAW welded specimen

Fig. 3.1 Configuration of welded specimen

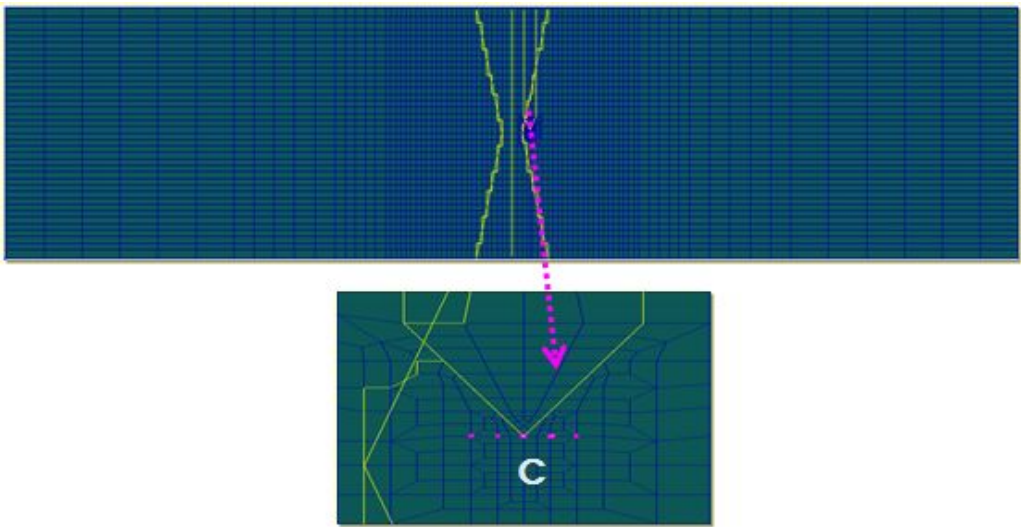

Fig. 3.2 FE model for numerical analysis

Table. 3.1 The chemical composition in EH36-TMCP and wire (Wt%)

Material	C	Si	Mn	P	S	Ni	Cu	Ti
EH36-TMCP	0.18	0.1~0.5	0.9~1.6	0.035	0.035	0.4	0.35	0.02
Wire for EGW	0.05	0.25	1.6	0.009	0.007	1.4	-	0.05
Wire for FCAW	0.04	0.38	1.10	0.012	0.010	1.55	-	-

Table. 3.2 The mechanical property in EH36-TMCP and wire

Material	Y.S(N/mm^2)	T.S(N/mm^2)	E.I(%)
EH36-TMCP	355	490~620	21
Wire for EGW	500	615	25
Wire for FCAW	560	620	29

Table. 3.3 Welding condition of specimen for EGW

Process	Number of Pass (Total /2Pass)	Current (A)	Voltage (V)	Arc Time (s)	Speed (cm/min)	Interpass Temp (℃)	Heat Input (KJ/cm)
EGW (3G)	Top(1Pass)	400	42	1589	4.5	116	235.2
	Bottom(1Pass)	430	44	1310	5.5	162	206.4

Table. 3.4 Welding condition of specimen for FCAW

Number of Pass (Total / 37Pass)		Current(A)		Voltage(V)		Arc Time(S)		Interpass Temp(℃)	
Top	Bottom								
1	1	240	300	30	31	405	373	119	119
2	2	280	300	31	31	352	361	123	135
3	3	300	300	31	31	365	359	114	157
4	4	300	280	31	32	143	223	123	128
5	5	300	280	31	32	182	209	141	147
6	6	300	280	31	32	193	262	137	130
7	7	300	280	31	32	172	191	131	112
8	8	300	310	31	31	151	265	115	129
9	9	300	310	31	31	174	262	119	145
10	10	300	320	31	31	147	244	131	125
11	11	300	320	31	31	199	226	149	136
12	12	300	320	31	31	151	237	127	115
13	13	300	320	31	31	201	246	139	118
14	14	260	320	29	31	131	212	152	124
15	15	260	320	29	31	171	187	121	131
16	16	260	320	29	31	121	257	147	135
17	17	260	275	29	31	117	213	114	105
18	18	260	275	29	31	153	227	127	111
	19		275		31		176		125

3.2 Thermal characteristics of welding processes

In this chapter, welding heat distributions for ultra thick steel plates by the variation of welding process such as EGW and FCAW have been investigated to the crack induced point which has been provided on crack tip in accordance with the same condition of 3 point bending specimen by BS 7448, and the analyses have considered to the characteristics of each welding process which may be varied by the time elapsed.

3.2.1 Heat conduction of EGW

Where the Fig.3.3 shows the time elapsed temperature rising and cooling history at 31mm along thickness direction (y=31mm) in way of crack induced point, the temperature variation are shown to the weld metal, heat affected zone and base metal which are located respectively at 198mm, 210mm and 220mm to the breadth direction of welding bead.

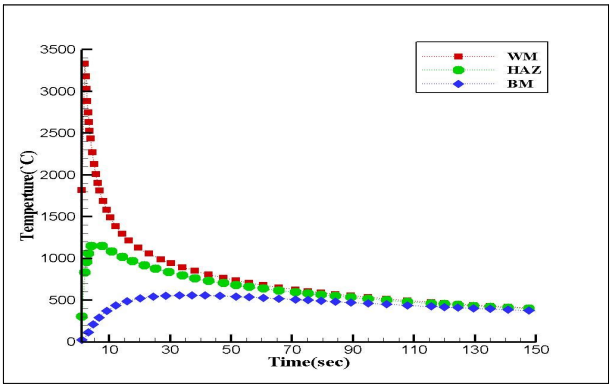

Fig. 3.3 Temperature history of WM, HAZ and BM in EGW

The highest temperatures after welding are reached by heat conduct when time elapsed is the 2 seconds on weld metal, 6 seconds on heat affected zone and 35 seconds on base metal. After this period of welding, each location at 110 seconds is cooled down to similar level in temperature gradient and contour.

Fig.3.4 (a) and (b) show the temperature history on front first welding pass and on backward second welding pass by time elapsed in way of the crack tip. The concerned crack edges are experienced the temperature variation through 800 to 1,000℃ and these gradients are gradually decreased by the accumulated welding passes.

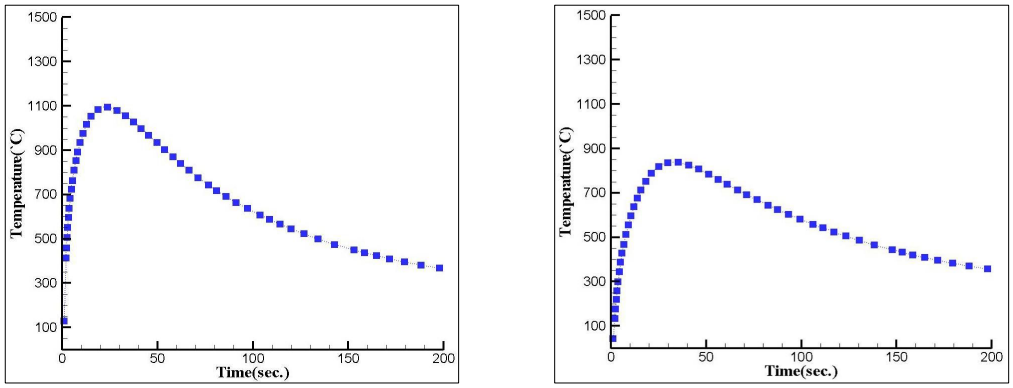

(a) 1Pass (b) 2pass

Fig. 3.4 Temperature history of crack tip in EGW

3.2.2 Heat conduction of FCAW

Where the Fig.3.5 shows the temperature rising and cooling stage at 31mm of thickness direction(y=31mm) when time elapsed, the temperature variation has described to weld metal, heat affected zone and base metal which were located respectively on 199.5mm, 206mm and 210mm to the breadth direction(x=199.5mm, 206mm, 210mm). As shown on the contour, the gradients of cooling temperature are very steeply decreasing and it is considered that the inputted heats are rapidly conducted to the ultra thick base metal, due to the less heat input then EGW. However, the temperature gradients and contours are reached to similar level after twentieth second of welding.

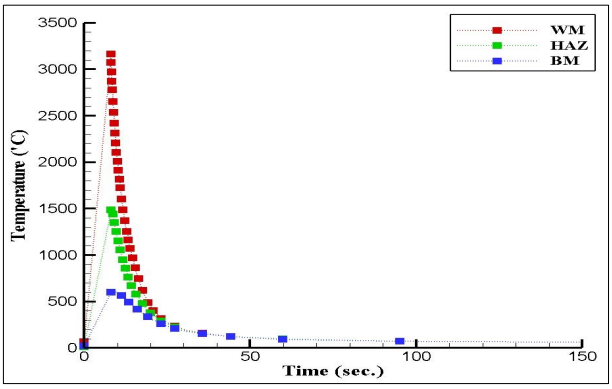

Fig. 3.5 Temperature history of W.M , H.A.Z and B.M in FCAW

Fig.3.6 (a) to (d) show the temperature history around concerned crack edge by each front & backward welding pass and the concerned crack edge experience temperature history between 750℃ & 1,400℃ in the highest temperature field and these temperature gradients tend to more easy by accumulating welding passes.

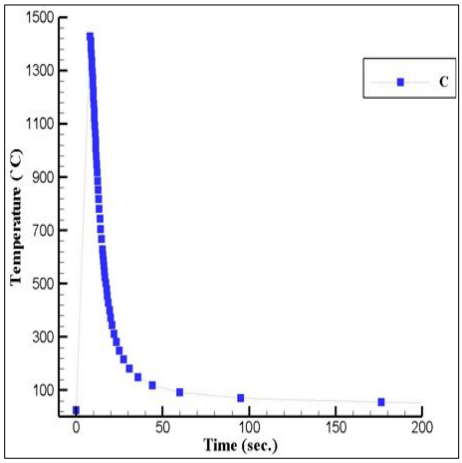

(a) 1 Pass (forward)

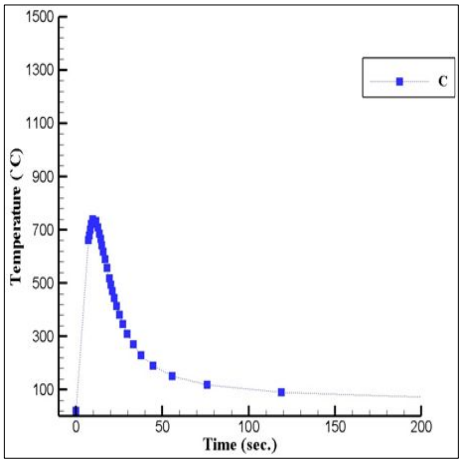

(b) 3 Pass (forward)

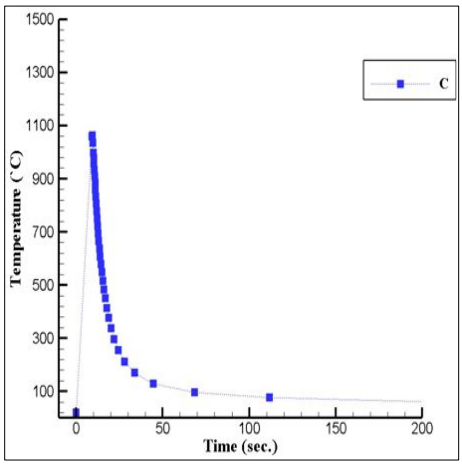

(c) 19 Pass (backward)

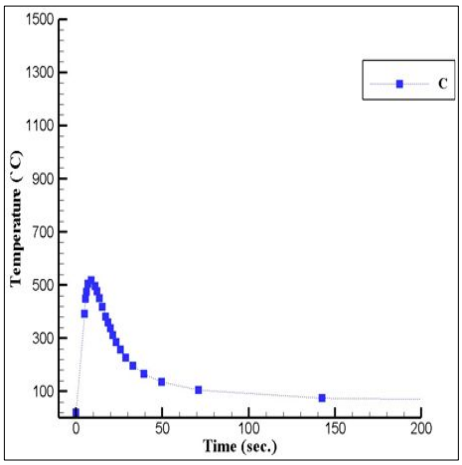

(d) 21Pass (backward)

Fig. 3.6 Temperature history of crack tip in FCAW

3.2.3 Discussion of heat conduction by welding processes

Compared with FCAW, the EGW shows that high temperature region is distributed widely. The temperature distributions for each welding process during the heating stage show that EGW is rapidly reached to the highest temperature than FCAW because of high heat concentration on the EGW, however, on the other hand the temperature on FCAW is cool down faster than EGW during the cooling stage, because of rapid heat conduction to the base metal. And thermal cycles by welding process in way of crack tip are similar as EGW experience more high temperature such as 800 through 1,300℃ while the FCAW experience the 750 through 1,400℃.

3.3 Mechanical characteristics of welding processes

In this chapter, the welding mechanism such as thermal stress and strain by thermal load which were produced due to the un-uniformed heat distribution as analyzed on chapter 3.3 will be considered.

3.3.1 Mechanical characteristic of EGW welding

FE model for this analysis is same with one used for heat conduction analysis and the plain strain thermal elastic-plastic analysis by FEM is conducted. Fig.3.7 (a) through (c) show the contours of welding residual stress to each direction X(σ_x), Y(σ_y) and Z(σ_z) throughout the FE model respectively. Fig.3.8 (a) to (b) show the distribution of welding residual stress X(σ_x) located on 35mm and 43mm to thickness direction for investigation of residual stress distribution in way of crack tip. As shown on these contours, the magnitude of each welding residual stress is in the order $\sigma_z > \sigma_x > \sigma_y$ and this result is caused by difference of mechanical restraints. Investigated the each welding stress, tensile σ_x and compressive σ_y are occurred on front side welding and large amount of compressive σ_z is distributed in way of center part of the specimen. In case of backward welding, all stress components are shown to tensile stress, center part of the specimen in particular, and it seems that large σ_z than one of the front welding is produced due to the restraint by former deposited welding i.e. front side welding. And the maximum equivalent stress produced on center layer of thickness direction is caused by high restraint which has been concentrated to center layer by welding heat input.

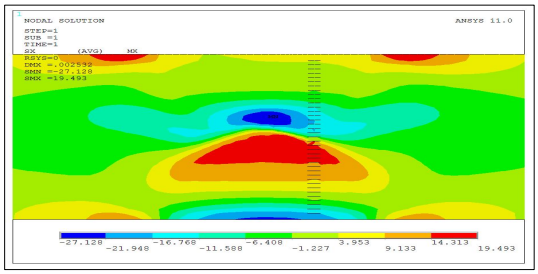

(a) σ_x

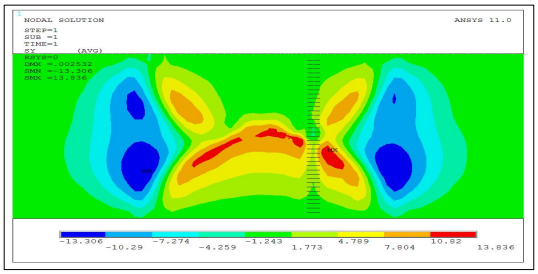

(b) σ_y

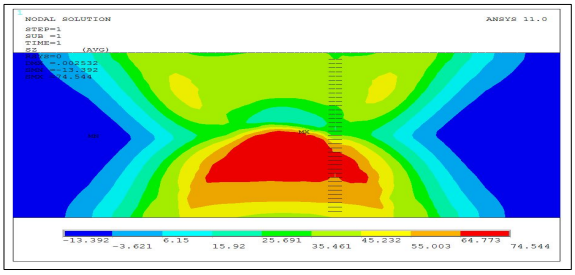

(c) σ_z

Fig. 3.7 Residual stress distribution of EGW welded specimen

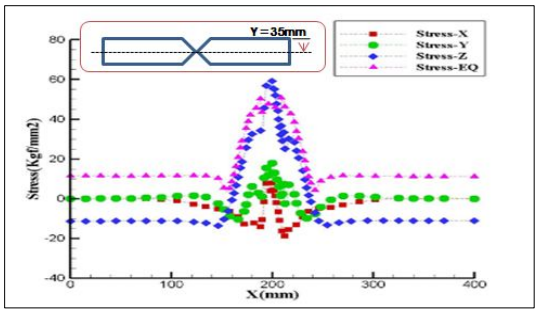

(a) Y=35mm

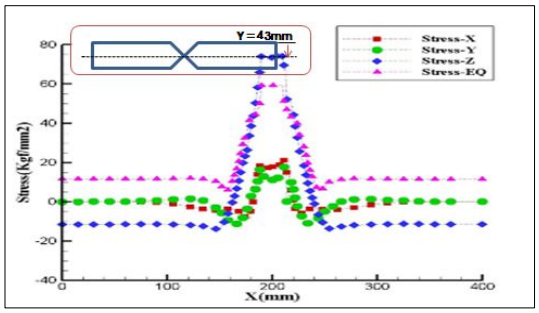

(b) Y=43mm

Fig. 3.8 Residual stress distribution of EGW welded specimen at different thickness locations

To investigate the effect of welding residual stress to fracture behavior in way of crack tip, the characteristics of distributed welding residual stress in way of crack tip are considered as shown Fig.3.9. As consequence of the review the welding residual stress(σ_x) on breadth direction, which will exert to fracture behavior such as crack opening-closure on crack tip, a tensile stress related to crack opening is occurred on crack tip, thus this tensile stress may influence seriously to crack opening even crack propagation, without further external load.

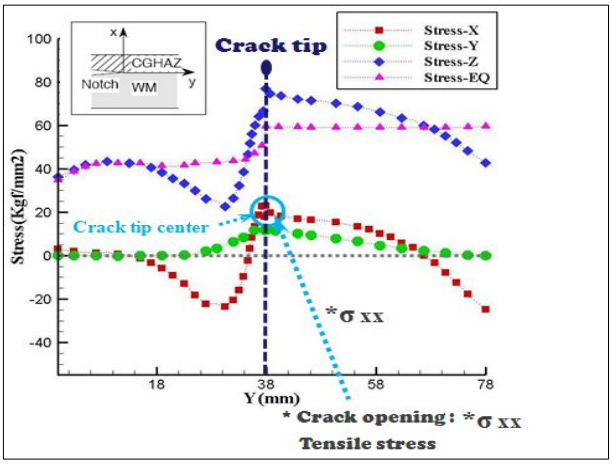

Fig. 3.9 Stress field near surface crack tip of EGW welded specimen

3.3.2 Mechanical characteristic of FCAW welding

Fig.3.10(a) through (c) show the contour of welding residual stress to each direction X (σ_x), Y(σ_y) and Z(σ_z) throughout the FE model respectively. Fig.3.11(a) to (b) shows the distribution of welding residual stress located on 19mm and 59mm to thickness direction.

As shown on these contour, the magnitude of each welding residual stress is in the order of $\sigma_z > \sigma_x > \sigma_y$. Considered the welding residual stress of former deposited welding has been released by heat input of later welding, the welding residual stress in the former welding region is decreased. But on contrary to this the residual stress in later welding part is increased by restraint of former deposited welding. And occurrence of maximum residual stress on specimen surface is caused by rapid temperature change due to the heat transfer from the surface.

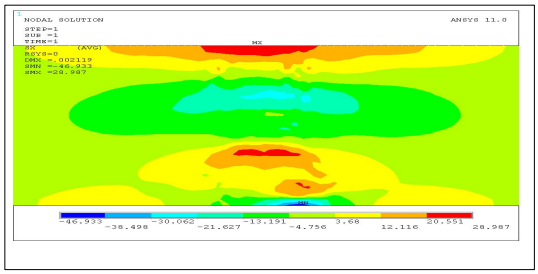

(a) σ_x

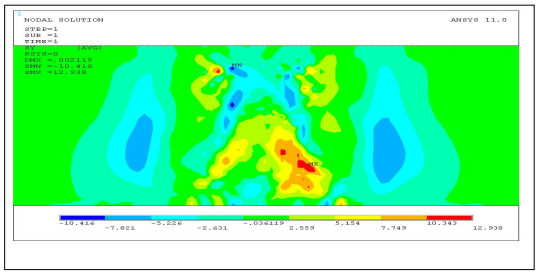

(b) σ_y

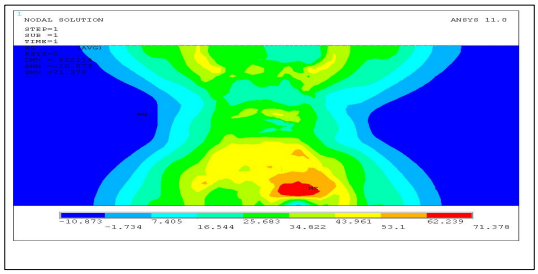

(c) σ_z

Fig. 3.10 Residual stress distribution of FCAW welded specimen

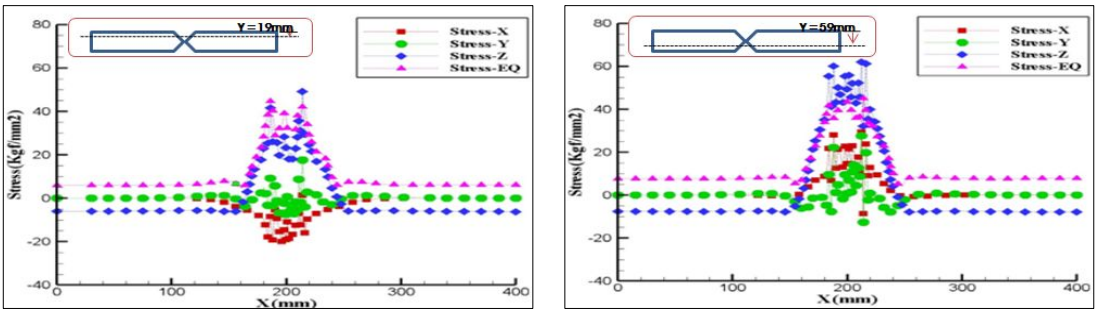

(a) Y=19mm (b) Y=59mm

Fig. 3.11 Residual stress distribution of FCAW welded specimen at different thickness locations

Fig.3.12 shows the welding residual stress on crack tip. Investigated the residual stress to breadth direction(σ_x) among the residual stress, compressive σ_x (crack closure stress) is produced on crack tip and this means that this compressive stress may influence to prevent or decrease the crack opening by closing the crack face even if a external force is not loaded.

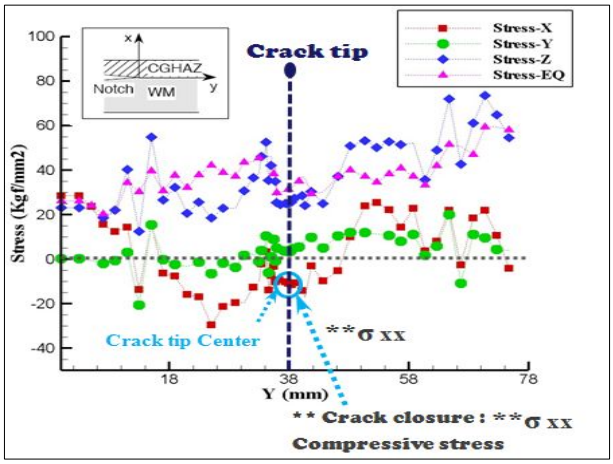

Fig. 3.12 Stress field near surface crack tip of FCAW welded specimen

3.3.3 Discussion of mechanical characteristic by welding processes

The magnitude of each welding residual stress is in the order of $\sigma_z > \sigma_x > \sigma_y$ in both EGW and FACW. Because of released welding residual stress by later welding, the welding residual stress on former weld(front side) has been released, then the level of residual stress become decreased below than later welding region(backward side) in which, on the contrary, welding residual stress is increased by former deposited welding.

The contours of σ_x which is closely related to crack opening-closure show that the welding residual stress on crack tip is the tensile in EGW and compressive in FCAW respectively, which means that crack may be propagated in EGW while prevented in FCAW, without exerting external load.

3.4 Redistribution of welding residual stress by the external load

In this chapter, the stress distributions by the external bending load and superposition such as welding residual stress & external bending load have been compared and analyzed to investigate the redistribution characteristics of welding residual stress in EGW and FCAW respectively. The welding residual stress resulted by thermal elastic-plastic analysis has been used to find the characteristics as an initial stress for ANSYS FE solver. And the analytic specimens reflecting a notch and initial crack on CGHAZ have been used as same as 3-point bend test.

3.4.1 Residual stress distribution by notch

As same as 3-point bend test, a notch and initial crack have been made on CGHAZ on which the lowest toughness occurs, and the characteristics of stress distribution around notch and crack tip have been examined when applying the external load. Fig.3.13 and 3.14 show each stress such as σ_x, σ_y, σ_z before and after notch preparation and it is found that the distributions of welding residual stress are tensile around notch tip before providing notch, but the distributions for all residual stress components around notch tip changes to compressive residual stress after providing notch and this trend become gradually decreased away from notch tip. Especially, σ_x closely related to crack opening-closure changes to compressive stress after providing the notch, while tensile stress promoting the crack before providing the notch.

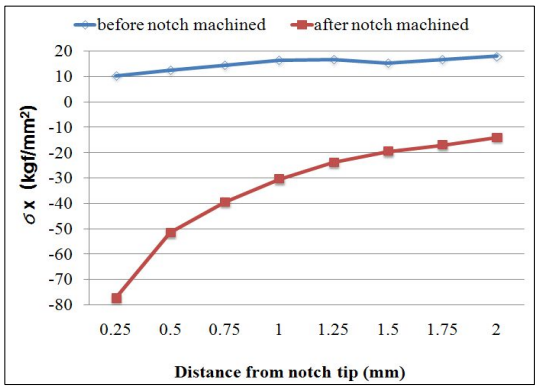

(a) σ_x

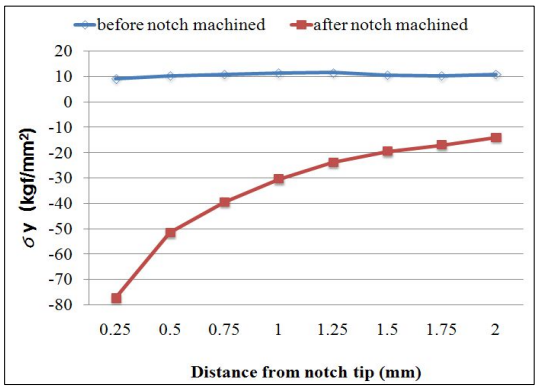

(b) σ_y

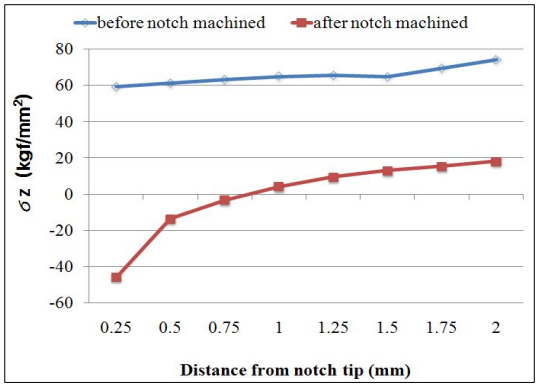

(c) σ_z

Fig. 3.13 Comparison of stress distributions ahead of notch tip in EGW welded specimen before and after notch machined

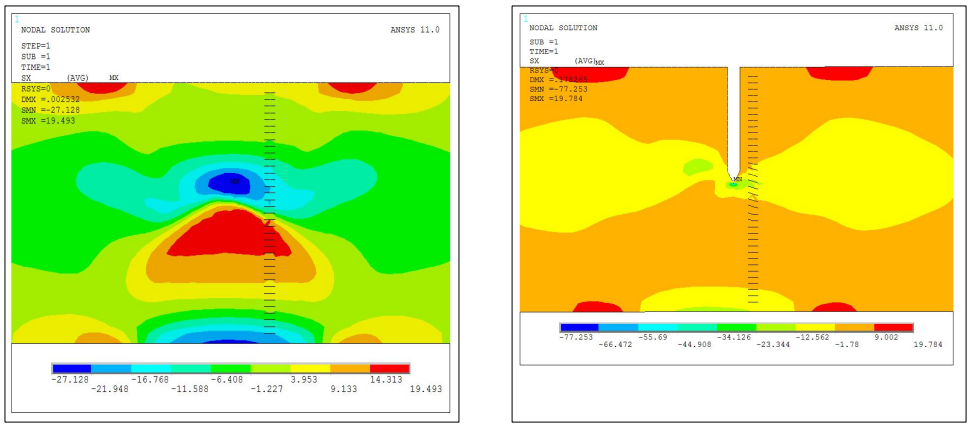

(a) σ_x

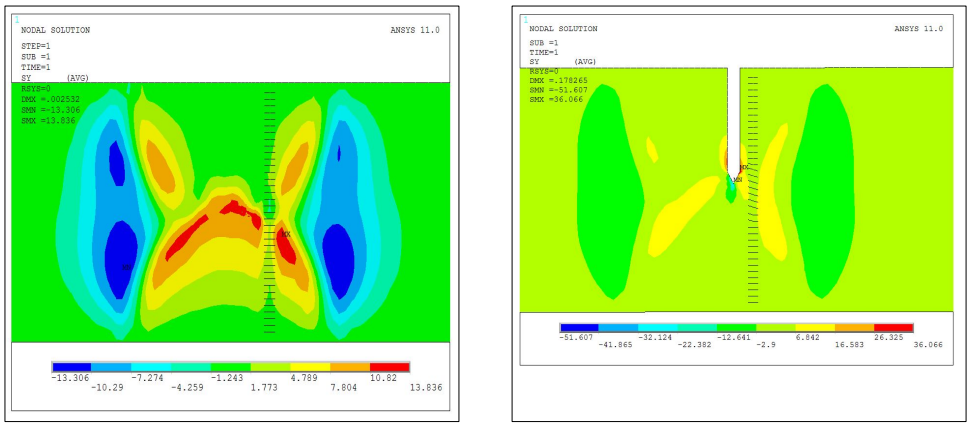

(b) σ_y

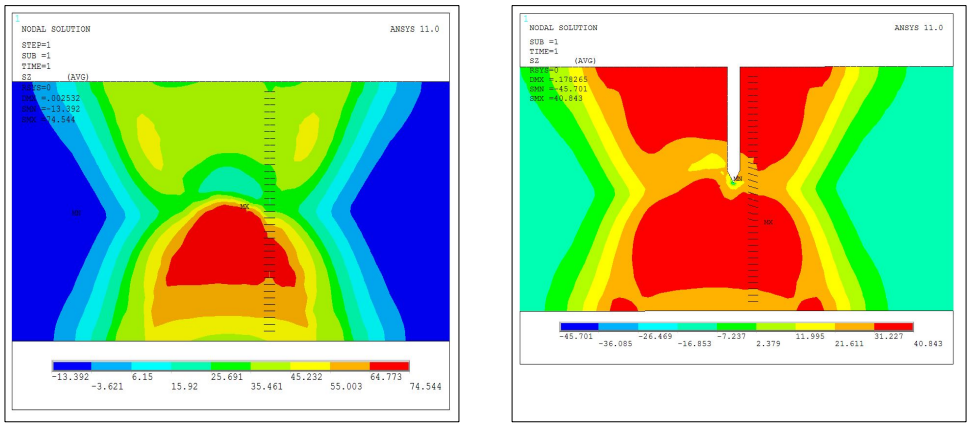

(c) σ_z

Fig. 3.14 Stress distributions ahead notch tip of EGW welded specimen before and after notch machined

Fig.3.15 and 3.16 show the residual stress distribution of FCAW at each location from the notch tip. As shown on these contours, σ_x and σ_y are increased or changed to compressive stress respectively while the value of tensile σ_z is decreased. And compressive σ_x, which is related closely to the retardation of crack opening, is increased sharply after providing the notch.

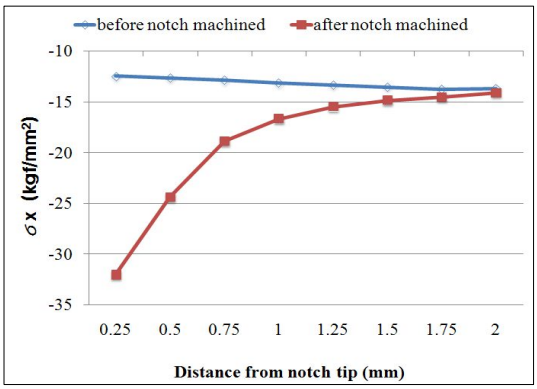

(a) σ_x

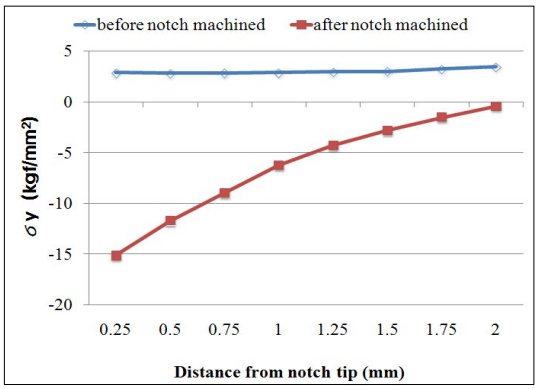

(b) σ_y

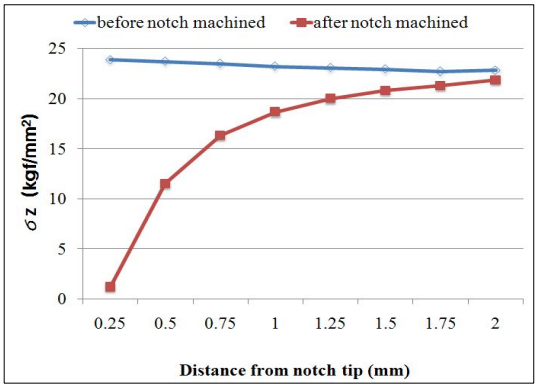

(c) σ_z

Fig. 3.15 Comparison of stress distributions ahead of notch tip of FCAW welded specimen before and after notch machined

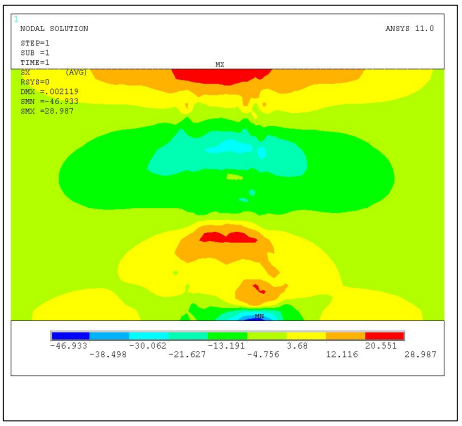

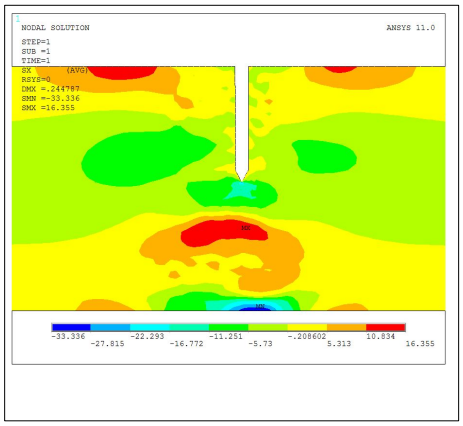

(a) σ_x

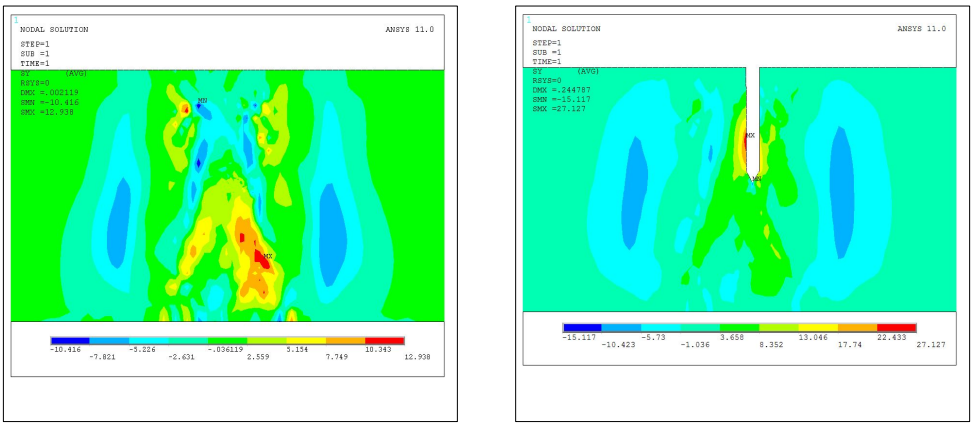

(b) σ_y

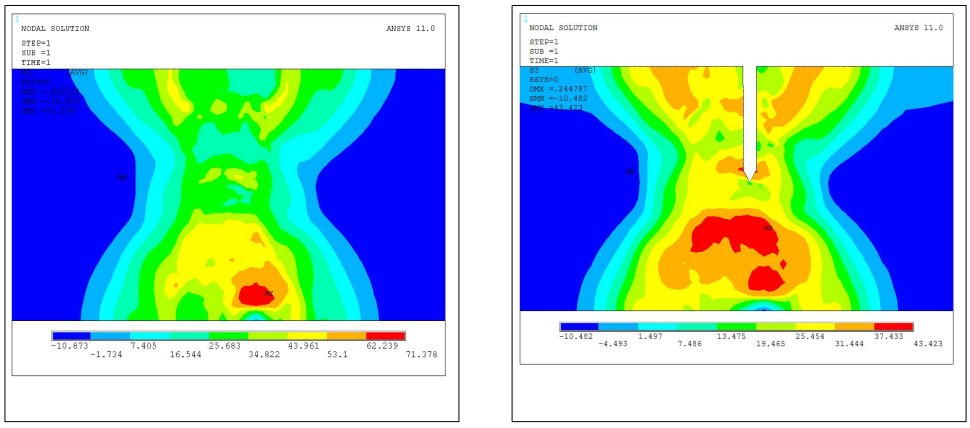

(c) σ_z

Fig. 3.16 Stress distributions ahead notch tip of FCAW welded specimen before and after notch machined

3.4.2 Residual stress distribution by initial crack length during the external bending load

To investigate the influence of superposition such as external bending force and existed welding residual stress by variation of initial crack length located on notch tip, the variation of stress distribution on crack tip have been examined at crack length a=38.25mm, 38.50mm, 38.75mm and 39mm. These crack length(a) means that the amount of length is added notch length and initial crack length which have been induced in accordance with BS 7448.

Fig.3.17 shows the stress distribution of EGW at each crack length when external bending force P_Q= 12,500kgf is applied. This external bending force, 12,500kgf, is originated by load-clip gauge displacement curves which has been analyzed to the fracture toughness K_{IC} as described on Chapter 4. As shown, the residual stress σ_x which will be exert mainly to crack opening is redistributed to tensile from compressive stress, and the stress on crack tip is increased as prolong the crack length but the aspect of stress distribution is distributed evenly.

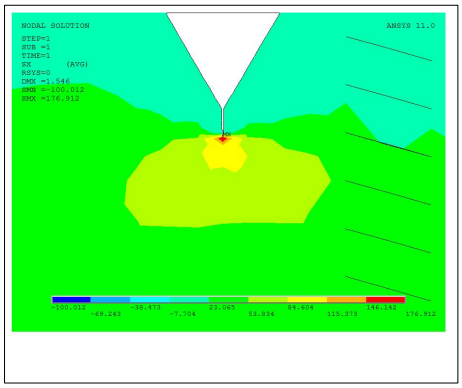

(a) a=38.25mm

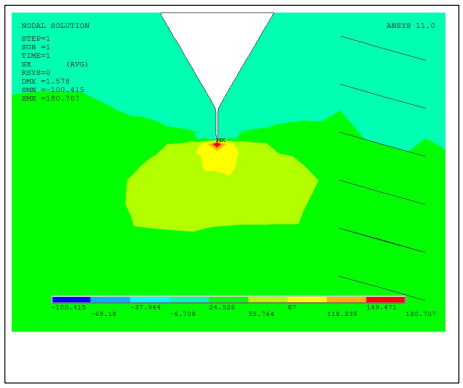

(a) a=38.50mm

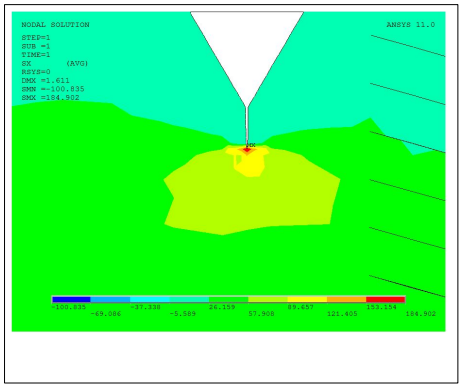

(c) a=38.75mm

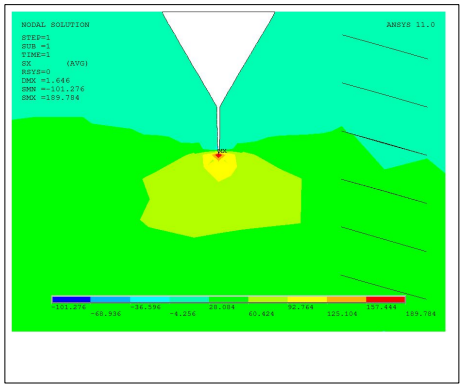

(d) a=39mm

Fig. 3.17 Redistributed residual stress(σ_x) of EGW welded specimen with crack length variation

Fig.3.18 shows the stress distribution of FCAW at each crack length such as a=38.25mm, 38.50mm, 38.75mm and 39mm, when external bending force P_Q= 13,000kgf is applied.

As shown, residual stress is redistributed to tensile from compressive stress by the bending force and the stress on crack tip is increased as prolong the crack length but the aspect of stress is distributed evenly. Compared the redistribution of stress between EGW and FCAW, compressive σ_x of FCAW which will exert to crack opening-closure is less than EGW in way of crack tip but this distribution become changed evenly as far from crack tip. Furthermore, the compressive residual stress σ_x and also equivalent stress of the FCAW in way of crack tip have been also distributed widely more than one of the EGW.

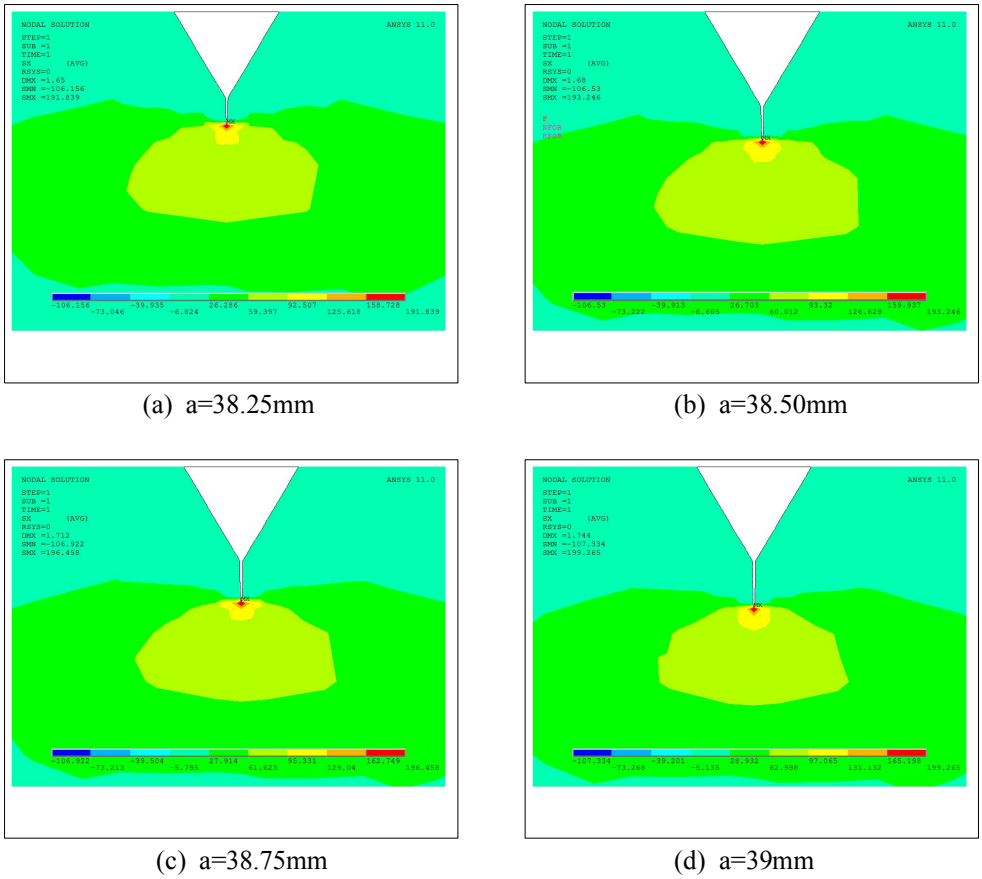

(a) a=38.25mm (b) a=38.50mm

(c) a=38.75mm (d) a=39mm

Fig. 3.18 Redistributed residual stress(σ_x) of FCAW welded specimen with crack length variation

3.5 Comparison an analytic result of FEM with experiment

As a result of measurements for the welding residual stress σ_x for EGW and FCAW as shown on Fig.3.19 to 3.20, the results are similar in qualitative side between FE simulation and experiment, even though the value of FEM is so higher than experiments.

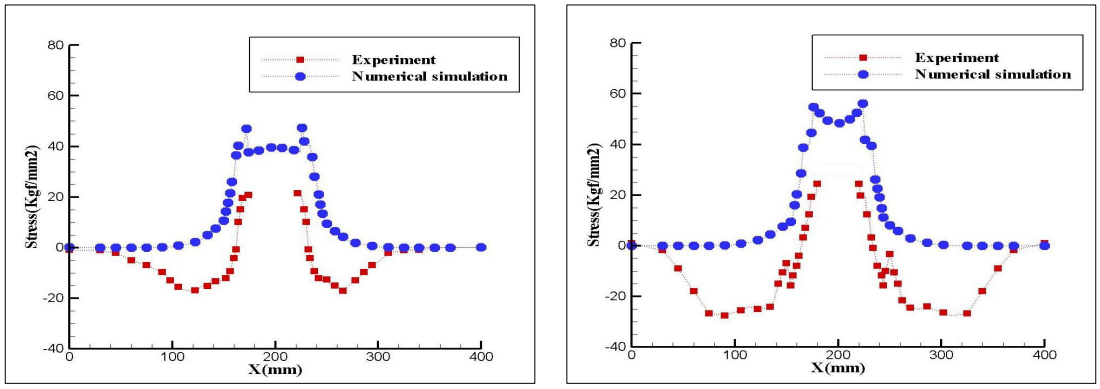

(a) Top side (b) Bottom side

Fig. 3.19 Comparison of welding residual stress values for EGW welded specimen

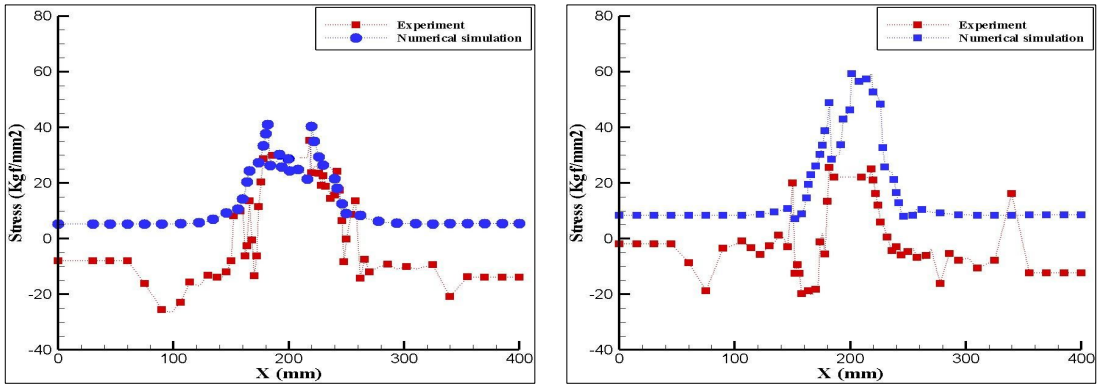

(a) Top side (b) Bottom side

Fig. 3.20 Comparison of welding residual stress values for FCAW welded specimen

Chapter 4. Assessment of plain strain fracture toughness K_{IC} in ultra thick steel plate (EH36-TMCP)

In this chapter, FEM analysis and fracture toughness K_{IC} for welding region, where a bending force and the superposition with bending & existed residual stress have been applied, are considered to predict the fracture toughness by each welding process, EGW and FCAW, in accordance with the variation of a/W.

4.1 FE model and analytic method

In accordance with BS 7448, FE model was chosen as same as the condition of 3 point bending experiment, and when external bending load applied the stress intensity factor at initial fracture point has been analyzed to the specimen after reflecting the notch and initial crack. Plain strain fracture toughness, $K_{IC,}$ means the lowest value to initiate the crack and the value can be calculated by the formula (4.1) on the basis of the load-clip gauge displacement curve when the crack propagation is reached to 2% of crack length.

$$K_Q = (P_Q S / BW^{2/3}) f(a/W) \tag{4.1}$$

where, B is specimen thickness, W is specimen width, a is crack length and S is distance between contents of rolls.

The crack-initiation point P_Q to calculate the K_Q is calculated by load-clip gauge displacement curve as described on Fig.4.1 and 4.2, which has been resulted by 3 point bending experiment and then the value of P_Q was satisfactorily confirmed with the formula (4.2).

$$\begin{aligned} P_{max}/P_Q \le 1.10 \quad & P_Q \text{ is valid} \\ P_{max}/P_Q > 1.10 \quad & P_Q \text{ is invalid} \end{aligned} \tag{4.2}$$

Then the stress intensity factor K_Q is calculated on the basis of calculated P_Q as a crack-initiation point and after an assessment of the validity to K_Q as described on (4.3), the K_Q is considered to K_{IC} as a plain strain fracture toughness:

$$B, a \geq 2.5(K_Q/\sigma_Y)^2 \tag{4.3}$$

Table. 4.1 shows the dimension, crack length and applied load(P) of FE model, to predict a fracture toughness of welding region by variation of welding process.

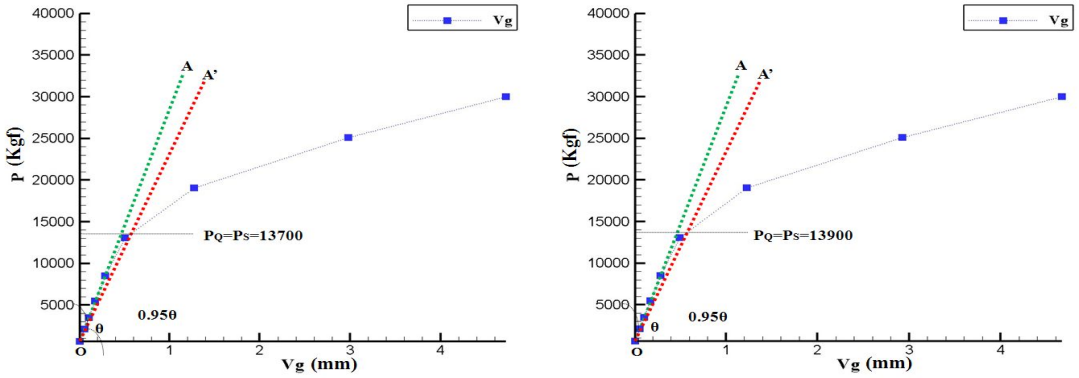

(a) EGW process (b) FCAW process

Fig. 4.1 Load-Clip gauge displacement curve for specimen considering only bending load in FEM simulation

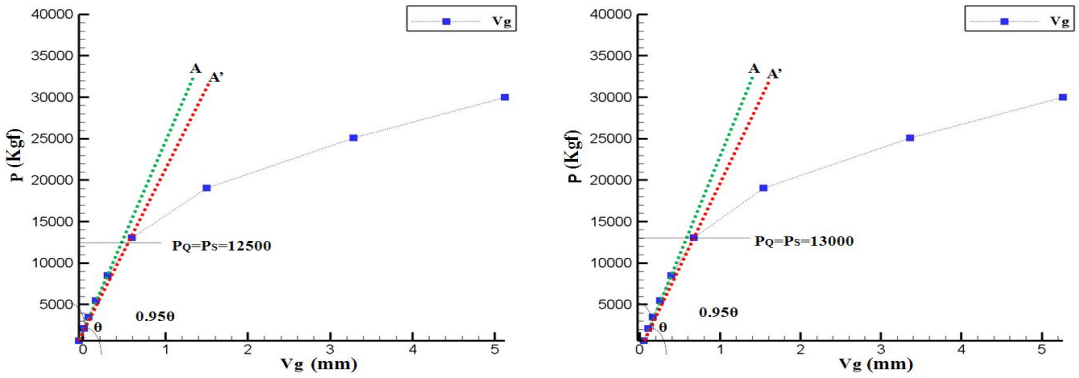

(a) EGW process (b) FCAW process

Fig. 4.2 Load-Clip gauge displacement curves for welded specimen considering superposition in FEM simulation

Table. 4.1 Numerical simulation condition used for fracture toughness K_{IC} prediction

Only load					
Specimen no.	Crack length(a:mm)	Specimen width(w:mm)	Specimen thickness(t:mm)	Load for EGW process(P_Q:kgf)	Load for FCAW process(P_Q:kgf)
1	38.25	78	78	13700	13900
2	38.50	78	78	13700	13900
3	38.75	78	78	13700	13900
4	39	78	78	13700	13900

(a) Numerical simulation condition for only load

Superposition					
Specimen no.	Crack length (a:mm)	Specimen width(w:mm)	Specimen thickness(t:mm)	Load for EGW process(P_Q:kgf)	Load for FCAW process(P_Q:kgf)
1	38.25	78	78	12500	13000
2	38.50	78	78	12500	13000
3	38.75	78	78	12500	13000
4	39	78	78	12500	13000

(a) Numerical simulation condition for superposition

4.2 Analytical result

Fig.4.1 (a) and (b) show the clip-gauge displacement curve for each welding process, related to resultant load and clip dislocation derived by 3 point bend test, when only bending load is applied without welding residual stress. The load P_Q at crack-initiation point is calculated from Ps which has crossed between the *OA'*, less than 5% from liner gradient *OA*, and Ps on load-clip gauge displacement curve. As shown on Fig.4.1, a load P_Q at crack-initiation point in EGW is 13,700Kgf and in FCAW is 13,900Kgf when considering only bending load.

On the Fig.4.2 for relations between resultant load and clip-gage dislocation when

superposition such as bending load and welding residual stress have been applied, (a) and (b) show the clip-gage displacement curve for the EGW and FCAW. As the equivalent loads to crack-initiation point P_Q are 12,500Kgf in EGW and 13,000Kgf in FCAW, the loads for applying the superposition are tend to decrease than only applying the bending load as described on Fig.4.1.

Table.4.2 and Fig.4.3 show the non dimensional stress intensity factor Fc by variation of a/W when a bending load and superposition with residual stress & bending are applied. Reviewed the non dimensional stress intensity factor Fc, the Fc value for the superposition is larger than only bending load while a/W is small, but the difference between superposition and only bending load is steeply decreased when the a/W increase. Especially, non dimensional stress intensity factor Fc on EGW is smaller than that of FCAW.

Table.4.3 to 4.4 show the fracture toughness value K_{1c} and K_{2c} by each welding process, EGW and FCAW, when a bending load and superposition with residual stress & bending are applied by variation of the a/W. Reviewed the K_{1c} and K_{2c} for EGW, the value of K_{1c} and K_{2c} are decreased or increased respectively when the a/W is small, but the K_{1c} and K_{2c} become similar when a/W is increased.

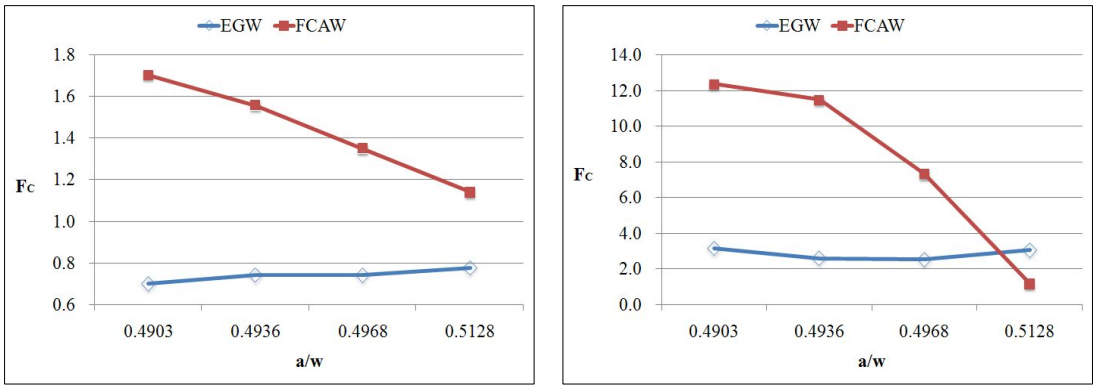

(a) Only load (b) Superposition

Fig. 4.3 Comparison of dimensionless stress intensity factors for crack under only load or superposition

Table. 4.2 Analysis results of dimensionless stress intensity factors Fc for welded specimens

Dimensionless stress intensity factor $(F_i = K_i / \sigma_{ij}\sqrt{\pi a})$								
EGW	Only load				FCAW	Only load			
	a/w	F_{1c}	F_{2c}	F_c		a/w	F_{1c}	F_{2c}	F_c
	0.4903	0.4247	-0.5568	0.7003		0.4903	0.4259	1.6499	1.7040
	0.4936	0.4245	-0.6079	0.7415		0.4936	0.4255	1.4983	1.5575
	0.4968	0.4251	-0.6073	0.7413		0.4968	0.4263	1.2810	1.3501
	0.5128	0.4259	-0.6494	0.7766		0.5128	0.4269	1.0583	1.1412
	Superposition					Superposition			
	a/w	F_{1c}	F_{2c}	F_c		a/w	F_{1c}	F_{2c}	F_c
	0.4903	0.4311	-3.1185	3.1481		0.4903	0.4205	-12.3617	12.3689
	0.4936	0.4298	-2.5544	2.5903		0.4936	0.4182	-11.4774	11.4850
	0.4968	0.4337	-2.4874	2.5249		0.4968	0.4181	-7.3060	7.3179
	0.5128	0.4340	3.0073	3.0384		0.5128	0.4195	-1.0814	1.1599

Fig. 4.5 for fracture toughness K_{IC} by variation of a/W shows that the K_{IC} value of EGW at superposition is less than at only bending load, and the difference of K_{IC} value for superposition at small a/W is larger than an application of bending load but this difference is gradually decreased. On the other hand, the K_{IC} value in FCAW is slightly increased for superposition at small a/W but as a/W increased the difference become similar.

Table. 4.3 Fracture toughness K_C on EGW welded specimens

Only load				
Specimen no.	a/w	K_{1C} (Kgf/mm$^{1.5}$)	K_{2C} (Kgf/mm$^{1.5}$)	K_{IC} (Kgf/mm$^{1.5}$)
1	0.4903	867.51	4.4019	867.52
2	0.4936	877.57	4.8215	877.58
3	0.4968	900.66	5.0868	900.67
4	0.5128	921.15	5.5497	921.17
Superposition				
Specimen no.	a/w	K_{1C} (Kgf/mm$^{1.5}$)	K_{2C} (Kgf/mm$^{1.5}$)	K_{IC} (Kgf/mm$^{1.5}$)
1	0.4903	836.19	32.640	836.83
2	0.4936	854.32	29.278	854.82
3	0.4968	884.94	27.845	885.38
4	0.5128	911.88	29.442	912.36

Table. 4.4 Fracture toughness K_C on FCAW welded specimens

Only load				
Specimen no.	a/w	K_{1C} (Kgf/mm$^{1.5}$)	K_{2C} (Kgf/mm$^{1.5}$)	K_{IC} (Kgf/mm$^{1.5}$)
1	0.4903	866.00	1.7521	866.00
2	0.4936	875.52	1.7529	875.52
3	0.4968	898.34	1.6495	898.34
4	0.5128	918.72	1.2491	918.72
Superposition				
Specimen no.	a/w	K_{1C} (Kgf/mm$^{1.5}$)	K_{2C} (Kgf/mm$^{1.5}$)	K_{IC} (Kgf/mm$^{1.5}$)
1	0.4903	884.31	4.8049	884.32
2	0.4936	889.00	0.65199	889.00
3	0.4968	906.39	4.6786	906.40
4	0.5128	925.32	2.0504	925.32

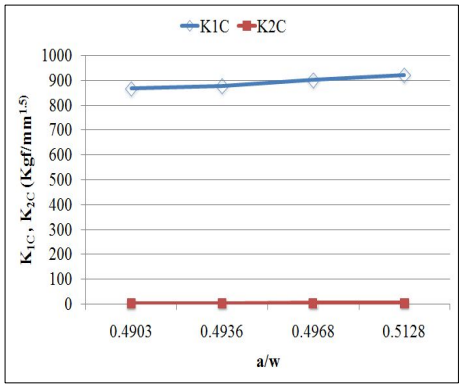

(a-1) EGW

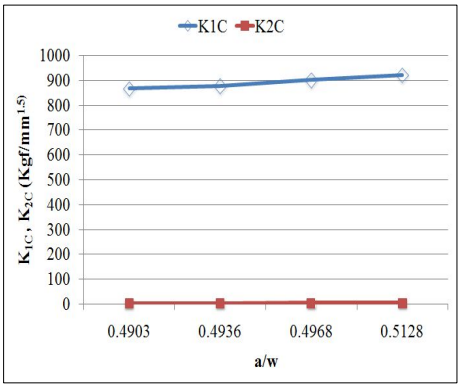

(a-2) FCAW

(a) Only load

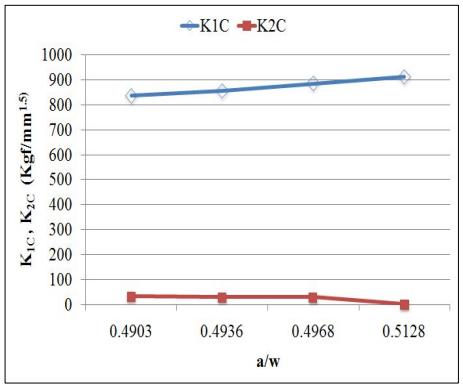

(b-1) EGW

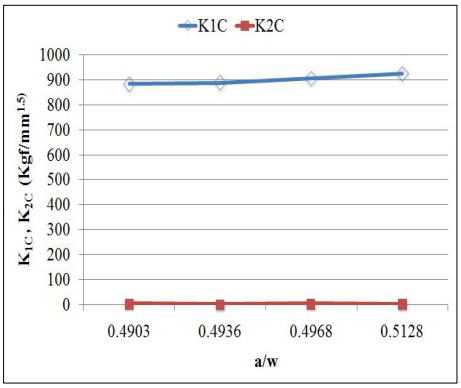

(b-2) FCAW

(b) Superposition

Fig. 4.4 Relation of stress intensity factors for crack under only load and superposition

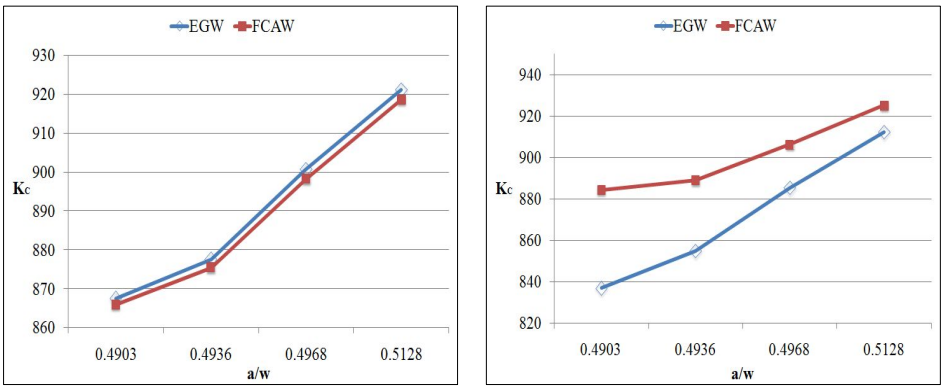

(a) Only load (b) Superposition

Fig. 4.5 Comparison of K_{IC} for EGW, FCAW welded specimens applied superposition with various initial crack length to width ratios

4.3 Comparison of plain strain fracture toughness K_{IC} by welding process

Fig.4.6 shows a fracture criterions for crack induced welding region by welding process. On the contrary to EGW, the fracture toughness of FCAW is increased at the superposition when the crack length is small, but this effect of residual stress is disappeared as the crack length is increased.

It is a well known fact that a welding structure is safe when the fracture toughness of that structure has low value, the EGW is more vulnerable to the propagation of crack than FCAW because of low fracture toughness value than FCAW but as this difference is very small it seems that each welding process such as EGW and FCAW will not affect to the fracture mechanics. Finally, it is concluded that a using the same fracture toughness criterion for these two welding processes is possible to conduct the establishment of fracture toughness criteria, prediction of the structural stability & fracture strength and assessment of fracture strength.

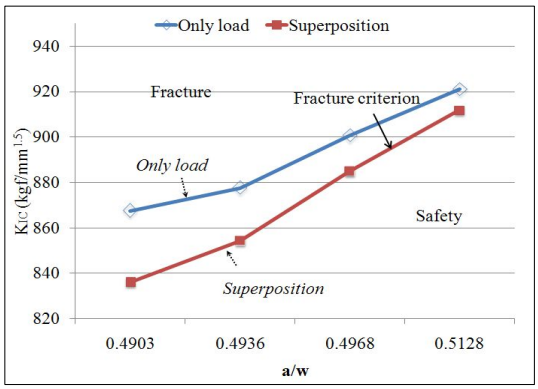

(a) EGW process

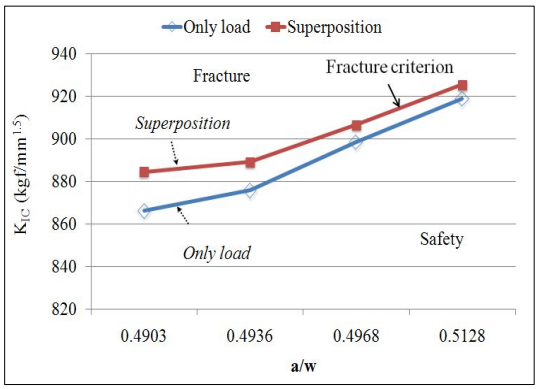

(b) FCAW process

Fig. 4.6 Comparison of K_{IC} for welded specimens with various initial crack length to width ratios

Chapter 5. The experimental assessment for mechanical behavior in EH36-TMCP by welding processes

5.1 Tensile test

As a result of tensile strength tests for EGW and FCAW, which has been conducted to half-thickness specimens, all specimens are fractured in way of base metal and the mean value of tensile strengths are measured to 540Mpa in EGW and FCAW, which are satisfied with relevant standard (min. 490Mpa) for EH36-TMCP as shown on Table. 5.1 and 5.2.

Table. 5.1 Tensile test for EGW

Item	Size (w×tmm)	Area(㎟)	Tensile strength	
			Total load(Ton)	Unit stress(MPa)
Spec.	-	-	-	490~630
1	25.0×40.2	1005.00	55.60	542.16
2	25.6×35.3	903.68	49.80	540.05
3	25.4×38.5	977.90	53.30	540.25
4	24.9×37.8	941.22	50.85	536.17

Table.5.2 Tensile test for FCAW

Item	Size (w×tmm)	Area(㎟)	Tensile strength	
			Total load(Ton)	Unit stress(MPa)
Spec.	-	-	-	490~630
A	25.3×38.0	961.40	52.60	536.17
B	25.3×37.5	948.75	51.30	529.89
C	25.3×37.3	943.69	51.95	539.48
D	24.9×37.8	941.22	52.25	555.13

5.2 Bending test

It is confirmed that side bend tests as shown on Table.5.3 and 5.4 are satisfied with relevant requirements such as classification rules.

Table. 5.3 Results of bending test for EGW

Item	Specimen Type	Angle	Requirement	Result
1~4	Side bend	180°	Open defect length≤ 3mm	Accepted

Table.5.4 Result of bending test for FCAW

Item	Specimen Type	Angle	Requirement	Result
1~4	Side bend	180°	Open defect length ≤ 3mm	Accepted

5.3 Impact test

Table. 5.5 to 5.6 show the value of absorbed energy which has been tested by charpy impact test at test temperature 40 degrees below zero. The test result shows that absorbed energy at each notch location of face & middle part such as weld metal, F.L, F.L+1mm, +2mm, +3mm, +5mm welding have a enough absorbed energy as more than 150J and these are satisfied with classification rules i.e. min. 34J in EGW and 47J in FCAW.

Table. 5.5 Impact test results for EGW

Notch Location	Specimen No.				Remark
	1	2	3	Avg.	
Weld Metal	146.6	148.6	163.4	152.9	Trans. Requirement 34J(at -20℃)
Fusion Line	313.1	210.9	280.6	268.2	
Fusion Line + 1mm	246.0	272.1	280.5	266.2	
Fusion Line + 2mm	231.0	337.1	325.7	297.9	
Fusion Line + 3mm	341.6	314.1	318.7	324.8	
Fusion Line + 5mm	328.0	299.8	316.4	314.7	

Table.5.6 Results of CVN impact test for FCAW

Notch Location	Specimen No.		Remark
	Face	Center	
Weld Metal	114.8	46.5	Trans. Requirement 47J(at -20℃)
Fusion Line	86.3	95.4	
Fusion Line + 1mm	186.4	301.2	
Fusion Line + 2mm	326.4	358.9	
Fusion Line + 3mm	308.5	297	
Fusion Line + 5mm	334.7	321	

5.4 Hardness test

This hardness test for each welding process by Vickers hardness Tester has been carried out throughout 22 points for weld metal, heat affected zone and base metal. Compared the hardness between front and backward welding regions, the value of backward is more high than front side. It was confirmed that test result are satisfied with classification requirement such as below 350Hv10 as shown Table. 5.7 & 5.8 and also this result is complied with mechanical properties of EH36-TMCP steel plate.

Table. 5.7 Results of hardness test for EGW

Hardness Value (HV10)										
1	**2**	**3**	**4**	**5**	**6**	**7**	**8**	**9**	**10**	**11**
206.5	174.4	185.6	175.0	215.4	215.6	209.2	191.7	187.8	190.1	214.9
12	**13**	**14**	**15**	**16**	**17**	**18**	**19**	**20**	**21**	**22**
210.4	199.3	204.1	218.1	232.2	235.6	236.4	207.2	216.9	212	211.1

Table. 5.8 Results of hardness test for FCAW

Hardness Value (HV10)										
1	**2**	**3**	**4**	**5**	**6**	**7**	**8**	**9**	**10**	**11**
194.8	217.9	212.9	207.9	212.0	218.5	218.2	231.4	223.8	210.2	190.9
12	**13**	**14**	**15**	**16**	**17**	**18**	**19**	**20**	**21**	**22**
186.4	229.6	240.6	241.6	204.5	225.2	220.7	232.6	225.3	222.6	198.8

Chapter 6. Analysis of CTOD on EGW and FCAW

6.1 Test specimen and condition for CTOD

As the CTOD(Crack Tip Opening Displacement) test is a measure to assess the structural stability by measuring the toughness on the basis of fracture mechanics theory, the CTOD test for EGW and FCAW are conducted in this chapter, in accordance with the BS 7448 standard. Even though any compulsory requirements of CTOD test has not settled in the ship construction, now some classification societies recommend that if the welding heat input and thickness of welding structure are more than 45kJ/cm and 50mm respectively, the welding structures need to be confirmed by CTOD or treated by post heat treatments.

Through many investigation and study in U.K since 1960 through 1970, the first CTOD test standard was published in Great Britain in 1979 under name of BS 5762. This original British CTOD test standard has been superseded BS 7448, which combined *K, J* and CTOD testing into a single standard. And several years later, American version of CTOD standard, ASTM E 1290 had been also published and then ASTM E1820 was published after combination of these three crack-tip parameters into a single standard.

As the Fig.6.1 shows the procedure for CTOD test by B x B 3-point bending specimen, the test procedure requires that a radius of the milled notch and band swan notch shall not excess a 0.1mm on radius and 0.15mm in breadth respectively. This means that if the dimension of specimen is not satisfied with the dimension requirements, the further test can not accepted, and also if the fatigue crack size including notch length exceeds 60% of breadth(W), which was fixed by specimen thickness(B), in the base metal and 70% in weld metal, the test will be invalidated.

During the test, a fatigue crack induced by 500ton class universal fatigue test machine is initiated with stress ration(R) 0.1. After completion of fatigue crack formation, the 3-point bending test is carried out after maintaining the temperature for 30 seconds, on condition that the specimen which was immerged in the refrigerant chamber with 10 degrees below zero and the temperature variation was not exceeded by 2 degree below and above.

During and after the test, a measurement of COD(Crack opening displacement) with Vp(plastic component of clip gauge displacement) & Pm value and evaluation of fatigue fractured surface & fatigue crack length(a_0) are conducted and the test procedure is described on Fig.6.1. Additionally, the fatigue crack length shall be complied with followings: first, the ratio to specimen's breadth (a_0/W) to be 0.45 to 0.55, second, the difference of crack length between any two sets of value to be not exceeded 10% of a_0, finally, a crack propagated angle from notch direction to be not exceeded 10°.

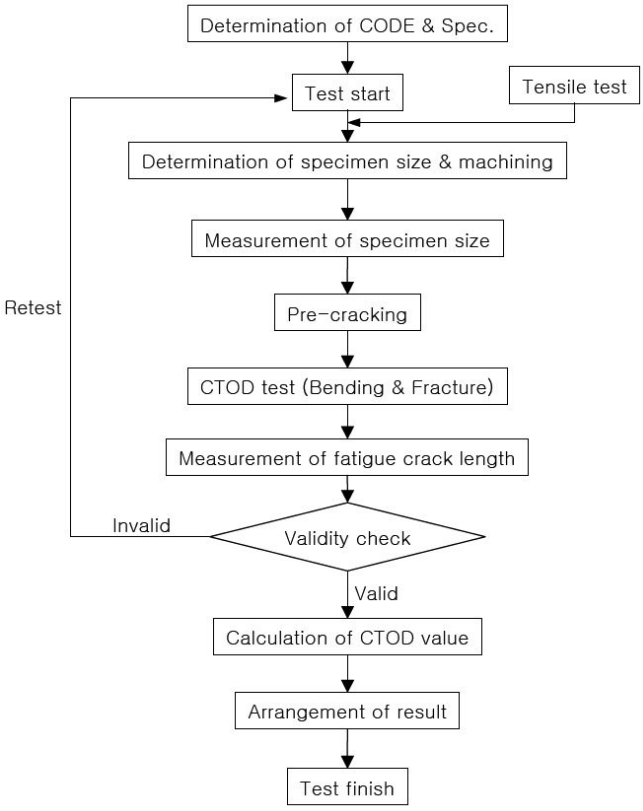

Fig. 6.1 CTOD test procedure

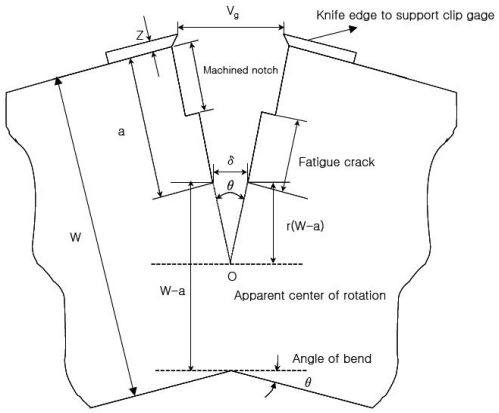

Fig. 6.2 Schematic diagram for CTOD values calculation

Among the several methods for CTOD test, an estimation method by displacement of clip gauge is used to in this study on the basis of rotating center. In this method, the specimen is supposed to the rotating rigid body on the r(W-a) as a central axis, located from crack tip, when bending load applied and by using relations between resultant δ and Vg, CTOD can be estimated as following formula:

$$\Phi = \frac{r(W-a)V_p}{a+z+r(W-a)} V_g \qquad (5.1)$$

where, r is rotation factor. In accordance with the BS 5762 for the 3 point bending test, CTOD(Ø) can be described on the r=0 as follows:

$$\delta = \frac{K^2(1-\nu^2)}{2\sigma_Y E} + \frac{0.4(W-a)V_p}{0.4W+0.6a+z} \qquad (5.2)$$

where, K = stress intensity factor

a = Effective crack length

Vp = Plastic component of clip gage displacement

z = Distance of clip gage location from test piece surface

Photo. 6.1 Universal testing machine

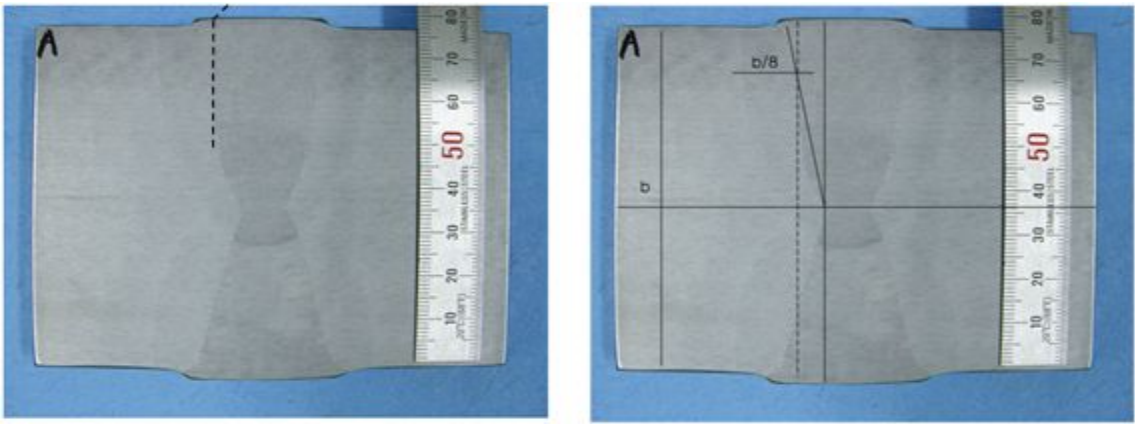

(a-1) Trough thickness notch (a-2) Surface notch

(a) Notch location of EGW welded specimen

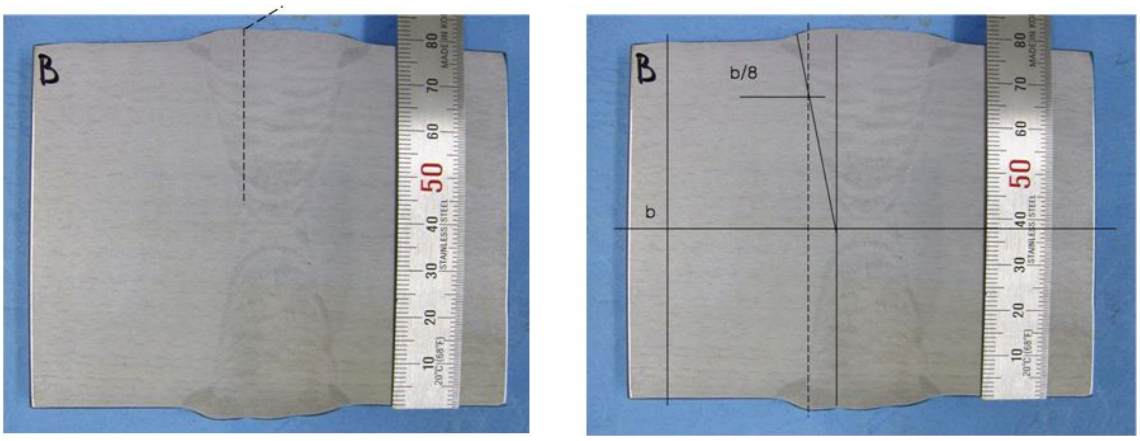

(b-1) Trough thickness notch (b-2) Surface notch

(b) Notch location of FCAW welded specimen

Photo. 6.2 Notch location of welded specimen

6.2 Evaluation of CTOD test by welding process

As Table. 6.1 shows the test result of CTOD, the CTOD values of EGW for the surface notch(1A) and through thickness notch(2A) which are located on CGHAZ are 0.212mm and 0.687mm respectively while the values of FCAW are 0.403mm(1B) and 0.939mm(2B).

The CTOD value in FCAW is higher than that of EGW and the values on surface notch in which the micro-structure is weak at crack tip is less than those of through thickness notch.

Table. 6.1 CTOD test results

Welding process	Location of Crack	CTOD value
A-EGW	**1A**-surface notch	**0.272**
	2A-through thick notch	**0.687**
B-FCAW	**1B**-surface notch	**0.403**
	2B-through thick notch	**0.939**

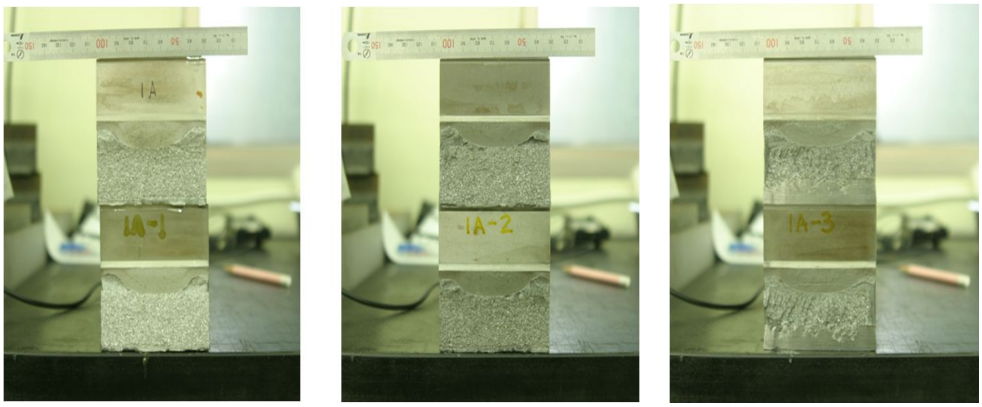

Photo. 6.3 Fractured EGW welded specimen with surface notch

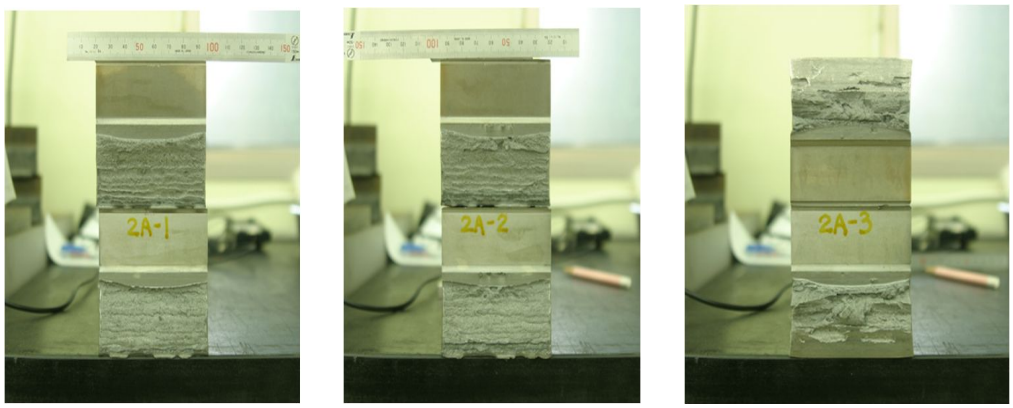

Photo. 6.4 Fractured EGW welded specimen with through thickness notch

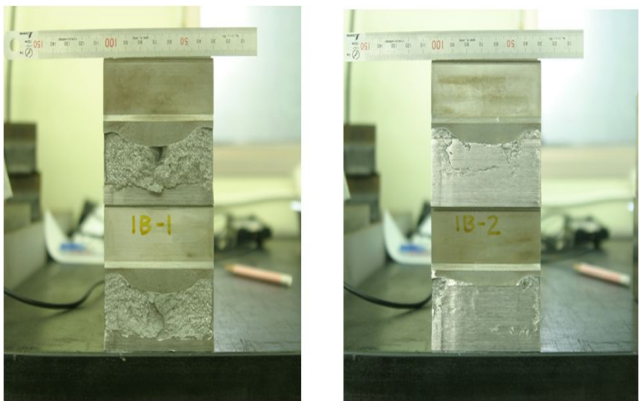

Photo. 6.5 Fractured FCAW welded specimen with surface notch

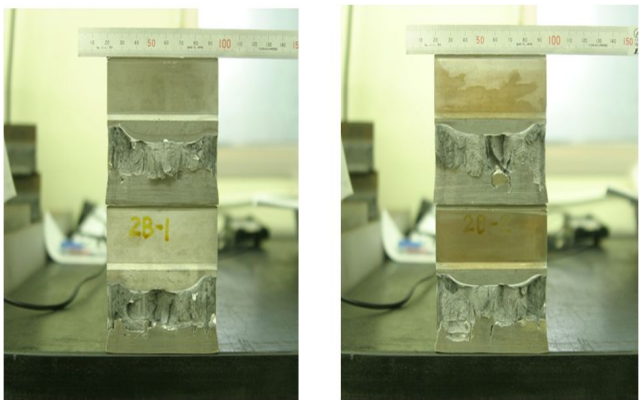

Photo. 6.6 Fractured FCAW welded specimen with through thickness notch

6.3 SEM of fatigue fractured surface in CTOD test

The evaluation of fatigue fractured surface after completion of CTOD test has been reviewed by SEM(Scanning Electron Microscope) as shown on Photo. 6.8 to 6.9. The shape of fracture face in EGW shows that the facet fracture is occurred as having a plain surface on fractured face while the FCAW shows the facet fracture together with partial dimple fracture. These mean that FCAW shows the ductile fracture due to the low heat input and small grain boundary but EGW shows a cleavage fracture due to the high heat input, large granule and brittle. In case of EGW, the difference of fractured faces between surface and through thickness notch is not shown.

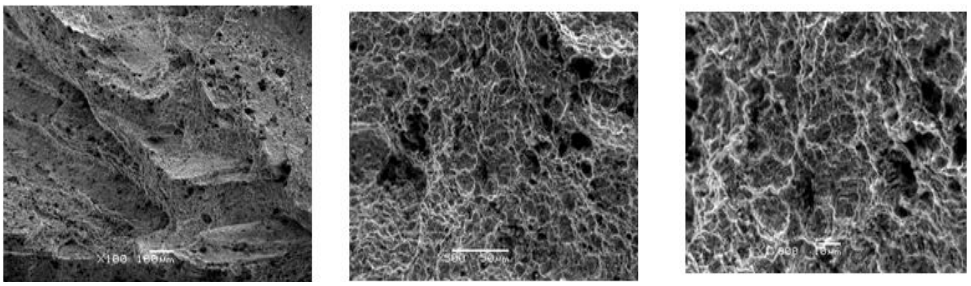

(a) brittle

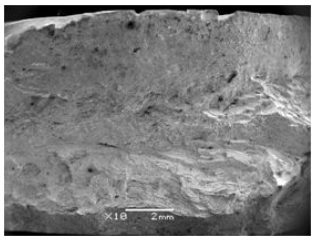

(b) Stretch zone

Photo. 6.7 SEM observation at fractured surfaces after CTOD test / FCAW welded specimen

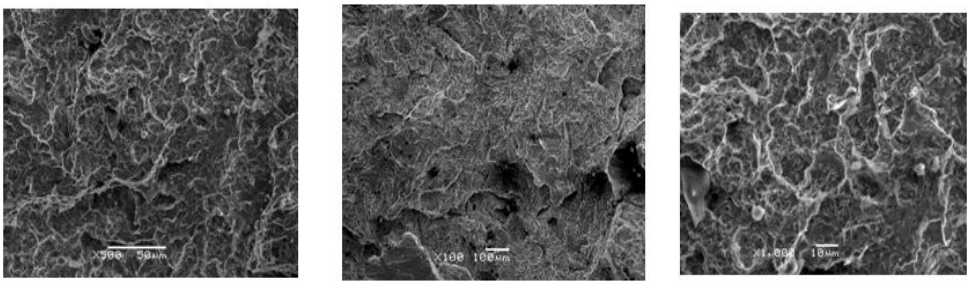

(a) brittle

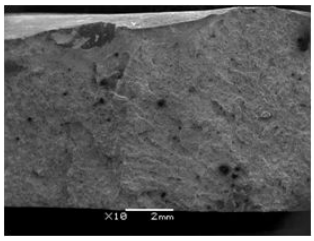

(b) Stretch zone

Photo. 6.8 SEM observation at fractured surfaces after CTOD test / EGW welded specimen

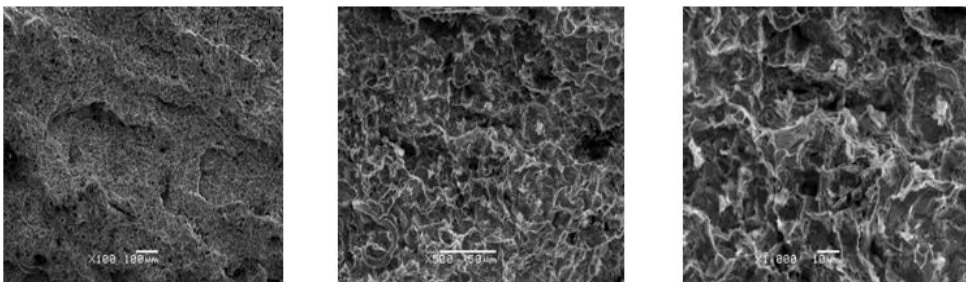

(a) brittle

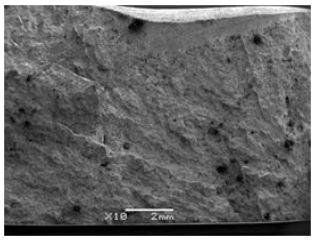

(b) Stretch zone

Photo. 6.9 SEM observation at fractured surfaces after CTOD test / EGW welded specimen

Chapter 7. Conclusions

Acknowledged the important of safety and economical benefit to use the ultra thick steel plates, EH36-TMCP, for offshore welding constructions, large sized ships and other relevant industrial parties, this study has carried out the theoretical analyses regarding the thermal conduction, mechanical behaviors by welding residual stress, effect of notch and external load, fracture toughness and the experimental confirmation by measuring residual stress, mechanical tests and CTOD test. Followings are the resultants of the analyses and experiments to investigate the structural stability and integrity of EGW welded joint, compared with FCAW.

1) Temperature distributions between EGW and FCAW are similar except maximum degrees of experienced temperature and the aspects of thermal distribution, because that the difference of inputted heat and sequence of welding layers.

2) Maximum residual stresses of EGW welded joint are distributed more widely than that of the FCAW and these trends are similar in way of crack tips. Welding residual stresses(σ_x) in EGW, which is closely related to crack opening-closure behavior are shown to tensile residual stress on the notch tip while that of FCAW is shown to compressive residual stress. These distribution of tensile residual stress in way of crack tip mean that a crack can be closed without any external force in FCAW, on the other hand the notch tip in EGW can be opened on that external load.

3) As the distributions of welding residual stress are changed when the notch machined to the specimens, the contours of residual stress(σ_x) in way of the notch tip have been changed to compressive from tensile residual stress in EGW while the contour of compressive residual stress(σ_x) in FCAW become larger than existing compressive residual stress. Even though the level of compressive residual stress(σ_x) at notch tip of FCAW is lower than that of EGW, the compressive residual stress in FCAW is distributed more widely than that of EGW, even the amount of equivalent stress on FCAW is also larger than EGW.

4) On applying the bending load to EGW and FCAW weld joints, a compressive residual stress(σ_x) at crack tip of notch is redistributed to tensile stress and the magnitude of the residual stress in front of crack tip are increased as the ratio to crack length(a/W) become large.

5) Compared the fracture toughness K_{IC} between EGW and FCAW welded joints, the K_{IC} of EGW welded joint is lower than that of FCAW, so it will be considered that crack propagation in EGW welded joint can be occurred easily. It is considered that the difference of values between EGW and FCAW is negligible as the difference in values are very small, however, the influence of difference value in fracture behaviors can be also disregarded.

6) Experimental result by mechanical test shows that the properties of welding specimens are satisfied with relevant classification rules and CTOD value of FCAW is higher than of EGW welded joint.

7) The result of SEM observation shows that fractured face in FCAW welded joint is subjected to ductile fracture while that of the EGW is subjected to cleavage fracture.

In the view of the structural integrity and stability for the welding construction which use ultra thick plate, the result of this study shows that large heat input welding such as EGW is complied with relevant requirements, and comparing with traditional welding process, FCAW, the EGW weld joint is also compatible with the large welding constructions.

Considering the main concern of the large heat input welding into high strengthen ultra thick plates is the crack susceptibility and possible crack propagation, the result of this study is very encouraged to use large heat input welding, EGW, in the view of the safety together with economical benefit. However, as demonstrated on this study, the accompanying affects such as more brittleness & less crack toughness than ordinary multi-layer welding process are inevitable to use the high strengthen ultra thick steel plate during the large heat input welding. Thus, through continuous improvement of compatible welding procedures need to be progressed together with development of steelmaking process.

REFERENCE

1. D. J Park, H. Kim, K. C. Nam, "An empirical study on the economical benefit of space chartering", Journal of Korean Navigation and Port Research 30(8), 2006, p663-668
2. C. G. Kim (2002), "A Study on the Trend and its limitation of Building Large Container Ship to reduce the logistics cost", The Korean Association of Shipping and Logistics, 2002
3. http://www.intport.org/html/sub2_2.html
4. Chaug-Ing HSU, Yu-Ping HSIEH, "Shipping Economic Analysis for ultra large container ship", Journal of the Eastern Asia Society for Transportation Studies, Vol. 6, 2005, p936 - 951
5. K. K. Um, S. H Kim, et al., "High Performance Steel Plates for Shipbuilding Applications", Proceedings of the Eighteenth (2008) International Offshore and Polar Engineering Conference, Vancouver, BC, Canada, July 6-11, 2008
6. S. H. Kim, I. S. Suh and K. B. Kan, "Development of TMCP Steel Plate For Shipbuilding Application", Posco Technical Report, Vol.10, No. 1, 2006
7. S. Suzuki, R. Muraoka, et al., "Steel Products for Shipbuilding", JFE Technical Report, No. 2, March 2004
8. M. Minagawa, K. Ishida, et al., "390 MPa Yield Strength Steel Plate for Large Heat-input Welding for Large Container Ships", Nippon Steel Technical Report No. 90 July 2004, p7-10
9. K. Ssaki, K. Suda, et al., "Development of Two-electrode Electrogas Arc Welding Process", Nippon Steel Technical Report, No. 90, July 2004, p67-74
10. S. Suzuki, K. Ichimiya, et al., "High Tensile Strength Steel Plates with Excellent HAZ Toughness for Shipbuilding-JFE EWEL Technology for Excellent Quality in HAZ of High Heat Input Welded Joints", JFE Technical Report No. 5, March 2005
11. C. M. Kim, J. B. Lee and W.Y. Choo, "Characteristics of Single Pass Welds in 50kJ/mm of Heavy Thickness Shipbuilding Steel", Proceedings of The Thirteenth (2003) International Offshore and Polar Engineering Conference, May 25, 2003
12. J. S. Park, G. B. An, B. Y. Jung and J. B. Lee, "Effect of welding heat input on the crack arrestability of thick steel plate welds", Proceedings of the Eighteenth (2008) International Offshore and Polar Engineering Conference, July 6, 2008

13. H. C. Jeong, Y. H. Park, Y. H. An and J. B. Lee, "Mechanical Properties and Micro structures of High Heat Input Welded Tandem EGW Joint in EH36-TM Steel", The Korea welding and joining society No.1(25), Feb. 2007
14. Offshore Technology Report for Steel, Health and Safety Executive, No.15, 2001
15. Fabrication and Testing of Offshore Structure , Offshore Standard, DNV-OS-C401, Oct. 2009
16. H. S. Bang, "Study on the mechanical behavior of welded part in thick plate - Three-dimensional thermal elasto-platic analysis based on finite element method", Journal of the Korean Welding Society 10(4) 1992, p37-43
17. Y. C. Kim, T. Yamakita, H. S. Bang, Y. Ueda. "Mechanical Behavior on Welding Residual Stress Relief Annealing of Repair Welding in Thick Plate". Q.J. Japan Weld. Society 6(1)1988, p53-59
18. Y. Ueda, Y. C. Kim, K. Garatani, T. Yamakita, H. S. Bang, "Mechanical Characteristics of Repair Welds Thick Plate - Distributions of Three-Dimensional Welding Residual Stresses and Plastic Strains and Their Production Mechanisms, JWRI 15(2) 1986, p359-368.
19. H. S. Bang, S. J. Kim, et al, "Study on lamellar tearing generated by corner joint welding in box column of ultra thick plate", Science and Technology of Welding & Joining 6(4), 2001, p213-219
20. Y. Ueda and T. Yamakawa."Analysis of Thermal Elastic-Plastic Stress and Strain during Welding by Finite Element Method ."Transactions of the Japan Welding Society 2(2)1971, p186-196
21. Lindgran, L. E, H. Runnemalm, et al., "Simulation of multipass welding of a thick plate", International Journal for Numerical Methods in Engineering 44(9), 1999, p1301-1316
22. Y. Ueda, K. Fukuda, SUZUKI " Transient and residual stresses from multipass welding in very thick plates and their reduction from stress relief annealing", Proc. 3rd Int. Conf. on Pressure vessel technology, Pt.II, p925-933
23. Mohamed Al-Shennawy, F. Minami, et al., "Crack-tip plastic constraint activators and application to plans-strain fracture toughness test: proposal on small-size fracture toughness specimen" Engineering Fracture Mechanics 63, 1999, p447-479
24. Ola Wall, "Numerical modeling of fracture initiation in large steel specimens at impact", Engineering Fracture Mechanics 69, 2002, p851-863
25. T. Inoue, T. Ishkawa, et al., "Long Crack Arrestability of Heavy-thick Shipbuilding steels", Proceedings of the Eighteenth (2006) International Offshore and Polar Engineering Conference, May 2008, p132-136

국문 초록

극후판 고장력강(EH36-TMCP)의 용접부 파괴인성에 대한 연구

조선대학교 선박해양공학과 김성주
지도교수: 방한서

용접구조물의 구조적 안정성 향상 및 이를 통한 경제적 이윤 증대를 위하여, 이들 용접구조물에 대한 철저하고 엄격한 안정성 평가와 작업관리는 구조물의 제작과정 및 운용과정에 발생할 수 있는 안전사고 예방의 측면은 물론 경제적 측면에서 필수 전제조건이다. 규모 경제로부터의 경제적 이익의 중요성을 감안하여, 현재 많은 대형 해상구조물, 대형 원유운반선(VLCC) 및 광석운반선(VLOC)은 물론 특히 콘테이너 선박의 건조가 증가하고 있으며 이러한 경향은 앞으로도 지속적으로 유지될 전망이다.

대형 콘테이너 선박의 경우 이러한 대형화는 현재 적극적으로 진행되고 있으며, 아울러 선박의 경하중량 감소와 종강도 향상을 위해 항복강도 355N/mm^2 이상 및 두께 70mm 이상의 고강도 후판의 사용 또한 급증하고 있다. 그러나 이러한 후판사용의 급증은 제작과정중 투입되는 노동력의 증가를 수반하며, 따라서 보다 효율적인 용접작업을 위해 기존의 다층용접 방법인 FCAW를 대체하는 용접방법으로서 EGW 등의 대입열 자동용접의 필요성이 대두되고 있다.

그러나 이러한 대입열 용접방법인 EGW의 적용은 기존의 다층용접방법인 FCAW에 비해 대입열에 따른 용접부의 취성증가 및 파괴인성 저하를 유발할 수 있으며, 따라서 본 연구에서는 기존의 FCAW 및 대체방안으로서의 EGW 용접방법의 각각에 대한 용접잔류응력 및 파괴인성에 대한 수치해석을 수행하여, 효율적인 용접방법으로서의 EGW 적용의 타당성 및 효율성 등을 검증하고자 하였다.

따라서 본 연구에서는 EGW 및 FCAW의 각 용접공정별 용접잔류응력 해석을 수행하였으며, 실제 용접구조물의 사용 환경조건을 고려하기 위해 기 해석된 용접 잔류응력에 기반하여 굽힘 외력 및 초기 균열을 고려하였을 때의 용접잔류응력의 재분포 특성을 해석하였다.

또한 대형 용접구조물의 안정성 확보 측면에서 필수적인 용접 파괴인성치를 해석하기 위하여, 균열진전의 시작점을 의미하는 지표로서 용접부의 파괴인성(K_{IC}) 해석을 각 용접 공정별로 수행하였으며, 해석수행 결과 FCAW의 파괴인성치가 EGW에 비교하여 더 양호한 결과를 나타내고 있음을 검증하였다. 그러나 이러한 용접 파괴인성치의 차이는 재료의 기계적 물성치에 비교하여 매우 적은 양으로서 결과적으로 그 차이를 무시할 수 있는 것으로 해석되었다.

용접후 재료의 기계적 특성 파악을 위하여 수행한 재료시험 결과에 따르면 시험결과가 동종 강(EH36-TMCP)에 대한 선급 규정치에 만족됨을 확인할 수 있었으며, 파괴인성 검증을 위해 영국 표준인 BS 7448에 따라 실시한 CTOD 시험결과 FCAW가 EGW와 비교하여 다소 양호함을 확인하였다. CTOD 시험후 재료 파면에 대해 실시한 주사전자현미경(SEM)을 통한 파면 확인결과 FCAW의 경우는 연성파괴를 EGW의 경우는 취성파괴의 현상을 각각 나타내고 있음을 확인하였다.

결론적으로 FCAW와 비교하여 EGW가 용접부 특성이 다소 취약하지만, 기존 다층 용접 방법인 FCAW의 대체 방안으로서 고강도 극후판(EH36-TMCP)에 대한 적용상 문제는 없는 것으로 검증되었다.

감사의 글

본 박사학위 과정완수를 위해 한결 같고 따뜻한 관심으로 성심을 베풀어 주신 방한서 교수님께 무엇보다 먼저 깊은 감사의 인사를 올립니다.

사회인으로서 학업을 병행하며 맞닿은 수많은 난관과 때로는 좌절의 순간에도, 새삼 포기하지 않고 오늘 새로운 박사학위 영예를 수여 받는 것은 지난 20여년전 처음 방한서 교수님을 만났던 꿈 많은 학부과정에서부터 인생의 동반자를 만나 가정을 꾸리는 결혼의 순간에도, 그리고 또다시 영예로운 박사과정을 마치는 지금까지 매 순간 곁에서 깊은 관심을 갖고 지켜 보아주신 방한서 교수님의 덕분이라 믿어 의심치 않습니다.

깊은 존경과 함께 인생의 스승님으로서 지난 긴 시간 그러했듯이 앞으로도 오랜 동안 한결같이 함께 계시기를 바랍니다.

아울러, 논문 지도 과정중 많은 도움과 성심을 다한 방희선 교수께도 깊은 감사의 인사를 드립니다. 미더운 선배가 되도록 항상 노력할 것이며 앞으로도 많은 관심과 애정으로 함께 일할 수 있는 기회가 있기를 바랍니다.

이제는 친구 같은 사랑스런 선희와 어느덧 불쑥 자라버린 유진, 호영 그리고 막내 주영이와 기쁨을 함께하고 싶습니다.

찾아 뵐 때 마다 애틋한 아버지와 항상 기도하시는 어머니에게 깊은 감사를 드리며 항상 건강하시기를 오늘의 기쁜 소식과 함께 전해 올립니다.

다시금 올라선 한 걸음을 위해 많은 관심과 도움을 주신 방한서 교수님을 비롯한 모든 분들께 감사드리며, 주어진 영예를 도전의 기회로 활용토록 항상 열심히 정진할 것임을 약속드립니다.

저작물 이용 허락서

학 과	선박해양공학	학 번	10041107	과 정	박 사
성 명	한글: 김 성 주 한문: 金 成 柱 영문: Kim Seong-Joo				
주 소	전남 해남군 해남읍 남외리 14-1				
연락처	E-mail: sjkim@krs.co.kr				
논문제목	한글: 극후판 고장력강(EH36-TMCP)의 용접부 파괴인성에 대한 연구				
	영문: A study on the Welding Fracture Toughness of the ultra thick High-tensile Steel Plate(EH36-TMCP)				

본인이 저작한 위의 저작물에 대하여 다음과 같은 조건 아래 조선대학교가 저작물을 이용할 수 있도록 허락하고 동의합니다.

- 다 음 -

1. 저작물의 DB구축 및 인터넷을 포함한 정보통신망에의 공개를 위한 저작물의 복제, 기억장치에의 저장, 전송 등을 허락함.
2. 위의 목적을 위하여 필요한 범위 내에서의 편집과 형식상의 변경을 허락함. 다만, 저작물의 내용 변경은 금지함.
3. 배포·전송된 저작물의 영리적 목적을 위한 복제, 저장, 전송 등은 금지함.
4. 저작물에 대한 이용기간은 5년으로 하고, 기간종료 3개월 이내에 별도의 의사 표시가 없을 경우에는 저작물의 이용기간을 계속 연장함.
5. 해당 저작물의 저작권을 타인에게 양도하거나 출판을 허락을 하였을 경우에는 1개월 이내에 대학에 이를 통보함.
6. 조선대학교는 저작물 이용의 허락 이후 해당 저작물로 인하여 발생하는 타인에 의한 권리 침해에 대하여 일체의 법적 책임을 지지 않음.
7. 소속 대학의 협정기관에 저작물의 제공 및 인터넷 등 정보통신망을 이용한 저작물의 전송·출력을 허락함.

동의여부 : 동의(○) 반대( )

2010년 2월 1일

저작자: 김 성 주 (인)

조선대학교 총장 귀하